國 立 交 通 大 學

電機與控制工程學系

碩士論文

電力系統中電壓崩潰偵測與電壓調節之研究

STUDY OF VOLTAGE COLLAPSE DETECTION AND

VOLTAGE REGULATION IN A POWER SYSTEM

研 究 生：劉宏毅

指導教授：梁耀文　博士

中 華 民 國 九 十 三 年 七 月

電力系統中電壓崩潰偵測與電壓調節之研究

STUDY OF VOLTAGE COLLAPSE DETECTION AND

VOLTAGE REGULATION IN A POWER SYSTEM

研 究 生：劉宏毅　　　　　　　　Student：Hung-Yi Liu

指導教授：梁耀文　博士　　　　　Advisor：Yew-Wen Liang

國立交通大學電機與控制工程學系

碩 士 論 文

A Thesis
Submitted to Department of Electrical and Control Engineering
College of Electrical Engineering and Computer Science
National Chiao Tung University
in Partial Fulfillment of the Requirements
for the Degree of Master
in
Electrical and Control Engineering
July 2004
Hsinchu, Taiwan, Republic of China

中華民國九十三年七月

電力系統中電壓崩潰偵測與電壓調節之研究

研究生：劉宏毅　　　　　　　　指導教授：梁耀文 博士

國立交通大學電機與控制工程研究所

摘　　要

在本論文中，我們利用錯誤診斷濾波器設計一電壓崩潰的偵測方法。同時為了更進一步提升電力系統之電壓品質，我們利用可變結構控制法則設計一電壓調節器用以達到電壓調節的目的。此外，我們亦設計一負載估測器用以估測電力系統之負載變動，且在設計電壓調節器時，亦把負載的變動考慮進去，使我們所設計之電壓調節器有更好的調節能力。最後，我們把偵測電壓崩潰的機制引入我們所設計之電壓調節系統，提供電力系統一個安全、穩定且可靠的操作環境。

STUDY OF VOLTAGE COLLAPSE DETECTION AND

VOLTAGE REGULATION IN A POWER SYSTEM

Student: Hung-Yi Liu   Advisor: Dr. Yew-Wen Liang

Department of Electrical and Control Engineering
National Chiao Tung University

ABSTRACT

In this thesis, we present a means of the detection of voltage collapse in a power system based on the linear-based fault identification filter (FIDF) design technique. Moreover, in order to promote the voltage quality of power supply for secure operation of a power system. We employ Variable Structure Control technique to design the voltage regulator of a power system. In addition, a load estimator is proposed to provide the accurate load variation to the VSC voltage regulator to have better regulating capacity. Finally, we combine the prior designs to maintain a secure and reliable operation of the power system.

誌　謝

TABLE OF CONTENTS

LIST OF FIGURES

CHAPTER 1

Introduction

1.1 Motivation

Recently, the study of power system stability has attracted lots of attention [6,28,34]. Among the possible instabilities, a serious type is the so-called "voltage collapse" [1,2,8,9,17,32]. This kind of instability in a power system is characterized by an initial slow progressive decline and then rapid decline in the voltage magnitude [17]. The voltage collapse behavior has been reported to be attributed to the increase of power demand that results in the operation of an electric power system near its stability limit [8,17].

In 1988, Dobson and Chiang [9] have presented a mechanism for voltage collapse and introduced a simple power system model containing a generator, an infinite bus and a nonlinear load. They claimed that the voltage collapse behavior might occur around a saddle node bifurcation point [8,9]. Abed et al. [1,2,32] have reported the oscillatory behavior of a power system using Hopf bifurcation theory.

In addition to distinguishing the cause of voltage collapse, to detect such instability phenomena is also an important area of research. Traditional available methods have relied on utilizing system Jacobian matrix of power flow [4,16,21,37], by exploiting either its sensitivity by determining its vicinity to singularity or its eigenvalue behavior. These approaches have the drawback of time consuming computations. And with increased network size these Jacobian based methods will become very time consuming and therefore inappropriate for quick detection. Thus, the first goal in this thesis is to provide a means for quick detection of voltage collapse in the power system. Various techniques for fault detection of a control system have been developed (see e.g., [5,7]). Among these techniques, the so-called "fault identification filter" (FIDF) is one of the most effective [5,7]. The FIDF has been successfully applied to the detection of sensor fault [23], mobile robot [24] and compression systems [19]. In this thesis, we adopt the power system model proposed by Dobson and Chiang [9], and employ FIDF design technique to detect the voltage collapse. We will show how the FIDF may be used to detect the occurrence of voltage collapse in a power system without complex computations.

In practical, an efficient and reliable operation of power systems should have the property that the voltage and frequency should remain nearly constant. As is well known, the frequency of a system is dependent on active power balance while the voltage magnitude is dependent on reactive power balance [16,27]. From voltage stability analysis, we know that the lack of the reactive power in the power system may cause the voltage decrease, which may in the worst case lead to the voltage collapse. So, an important issue for power system control is to maintain a steady acceptable voltage under normal operation and disturbed conditions, which is referred as the problem of voltage regulation. Thus, the second goal in this thesis is to provide a voltage controller which can achieve voltage regulation purpose. Tap changer is

known to be one of an effective device for voltage control. The effect of tap changer ratio in the power system has been studied in [20,22,39,16,27]. In this thesis, we will employ setting tap changer ratio to achieve voltage regulation. In practical, the power systems are large scale nonlinear systems. The simplest controller design for voltage regulation might be based on approximate linearization approach. However, this controller is usually effective around a neighborhood of operating point. In addition, the linearization approach might work well when a small disturbance occurs, but it usually cannot survive a large disturbance. Recently, nonlinear control theories have been employed to power systems voltage controller design. These designs are mainly based on the nonlinear feedback linearization technique [10,33,38], which transforms the power system into a linear and controllable one, and thus linear control theories can be applied to design an effective control law. Although the feedback linearization approach is a powerful tool for nonlinear controller design, it is only suitable for nonlinear affine systems (for definition, see e.g., [3]). Since in this thesis we take the tap changer as control input, the power system model is found to be a general nonlinear system form $\dot{x} = f(x, u)$ in stead of being a nonlinear affine version. Thus feedback linearization approach can not be applied. It is known that variable structure control (VSC) has many advantages including fast response and small sensitivity to system uncertainties and disturbances [25,29]. It then has been widely applied to a variety of control problem, such as power system stability control [13,34,36], robotic control [15,26], and so on. In this thesis, we will adopt the VSC technique in the controller design issues.

In many practical control problems, the controlled systems usually have parameter uncertainty. The uncertainty in power system may come from a large variation in loading condition during operation. It is known that the performance of a control system might not be acceptable or even result in unstable if it does not take the

3

parameter uncertainty into account for controller design. Thus, the third goal in this thesis is to provide a parameter estimation scheme to help voltage controller dealing with the power system in the presence of uncertainty or unknown variation in the load.

Finally, we will develop a scheme of prevention of voltage collapse with the aid of prior analysis and design. It provides us a secure and reliable operation of the power system.

1.2 Outline

The organization of this thesis is as follows. In Chapter 2, we recall some basic tool and theory. These include Fault Identification Filter, short-time Fourier transform, Variable Structure Control, Adaptive Control. In Chapter 3, we first introduce the model of power system proposed by Dobson and Chiang [9]. Then, we apply the FIDF to the detection of voltage collapse in a power system. In Chapter 4, we establish the model of power system with tap changer. Then, the Variable Structure Control scheme is applied to adjust the tap changer ratio for the purpose of voltage regulation. In Chapter 5, a scheme of prevention of voltage collapse is proposed, and Simulation results demonstrate the effectiveness of this scheme. Finally, conclusions and suggestions for further research are given in Chapter 6.

CHAPTER 2

Preliminaries

In this chapter we review some basic tool and theory. These include Fault Identification Filter [5,18], short-time Fourier transform [11], Variable Structure Control [25,29], adaptive control [25]. These results will be employed in the next two chapters to develop the detection of voltage collapse and voltage regulation for the electric power system.

2.1 Fault Identification Filter (FIDF)

Fault Identification Filter is a tool that can provide an efficient approach to detect the appearance of faults in a control system. In this section we recall the FIDF design results presented in [5].

Consider a linear system is given by

$$\dot{x}(t) = Ax(t) + Bu(t) + E_1 f(t) \tag{2.1}$$

$$y(t) = Cx(t) + Du(t) + E_2 f(t) \tag{2.2}$$

where $x(t) \in \mathfrak{R}^n$, $u(t) \in \mathfrak{R}^m$, $f(t) \in \mathfrak{R}^q$, and $y(t) \in \mathfrak{R}^p$ denote the state vector, the

input vector, the fault vector, and the output vector, respectively. From (2.1) and (2.2),

by taking Laplace transform, we have

$$y(s) = G_u(s)u(s) + G_f(s)f(s) \tag{2.3}$$

where

$$G_u(s) = C(sI - A)^{-1}B + D \tag{2.4}$$

and

$$G_f(s) = C(sI - A)^{-1}E_1 + E_2 \tag{2.5}$$

The object of FIDF design is to obtain two proper and stable filters $H_1(s)$ and

$H_2(s)$ such that the residual vector

$$r(s) = H_1(s)u(s) + H_2(s)y(s) \tag{2.6}$$

has the following property :

$$r(s) \to 0 \quad \text{if and only if} \quad f(s) \to 0 \tag{2.7}$$

From Eqs. (2.3)-(2.6), we have

$$r(s) = [H_1(s) + H_2(s)G_u(s)]u(s) + H_2(s)G_f(s)f(s) \tag{2.8}$$

The configuration of a FIDF is shown in Figure 2.1.
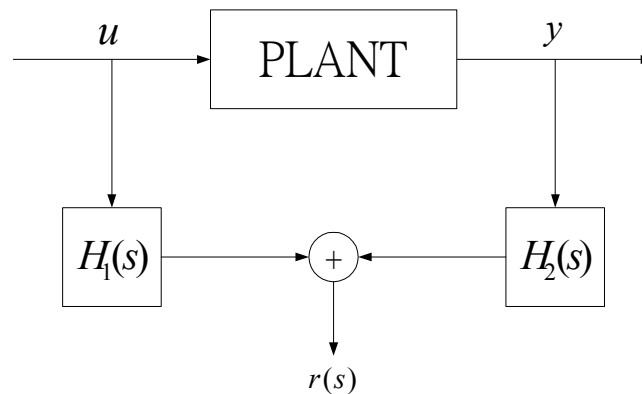
Figure 2.1: FIDF configuration

To fulfill the requirement of (2.7), we first assume that $G_f(s)$ as given by (2.5) is invertible. The FIDF design procedure is given in [5] then can be summarized as the following algorithm.

Algorithm 1 (FIDF design procedure)

Step 1 : Construct $H_2(s)$ so that the transfer matrix $H_2(s)G_f(s)$ is a diagonal proper

and stable one.

Step 2 : Determine $H_1(s)$ such that $H_1(s) + H_2(s)G_u(s) = 0$

Step 3 : Establish and check $r(s)$ according to Eq. (2.6)

Under the procedure of Algorithm 1, it is noted from Eq. (2.8) that the residual vector is influenced only by the fault vector. Thus, by properly checking the value of residual vector as listed in Step 3 of Algorithm 1 above, one can detect the system fault accurately. In addition to the effect of fault vector, the system output is also affected by nonzero initial state. Since the objective is that the residual be affected only by the fault vector, The response to a nonzero initial state should decay to zero. This implies that the matrix A in Eq. (2.1) should also be required to be stable.

2.2 Short-Time Fourier Transform

The short-time Fourier transform is the most widely used method for studying nonstationary signals. The concept behind it is simple and powerful. Break up the signal into small time segments and Fourier analyze each time segment to ascertain the frequencies that existed in that segment. That is the basic idea of the Short-time Fourier Transform. The totality of such spectra indicates how the spectrum is varying in time.

2.2.1 Window function

If we are interesting in a desired portion of a signal at time t, it can be obtained by multiplying the original signal by a window function, which emphasizes the signal at that time interval, centered at t, and suppresses the signal at other times.

Let $\phi(t)$ be a real-valued window function. Then we apply the window function to the original signal and obtain the information of $f(t)$ near $t = b$, and express this as $f(t)\phi(t-b) =: f_b(t)$. In particular, if $\phi(t) =: \chi_{[-\tau,\tau)}(t)$, as shown in figure2.2, then

$$f_b(t) = \begin{cases} f(t), \ t \in [b-\tau, b+\tau) \\ 0, \qquad otherwise. \end{cases} \tag{2.9}$$

where b is a sliding factor and we can slide the window function along the time axis to analyze the local behavior of the function $f(t)$ in different intervals.
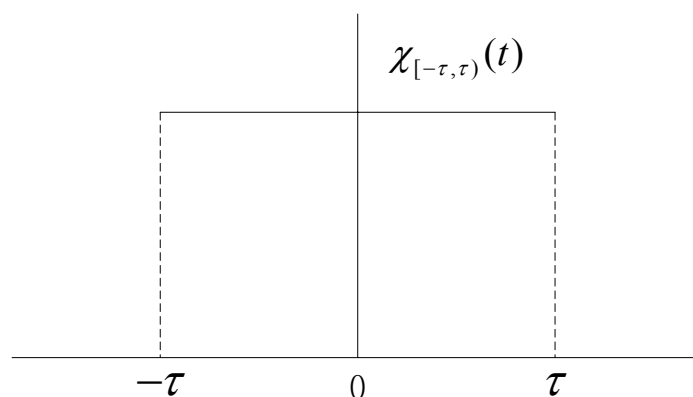
Figure2.2: Characteristic function

In the window function, We have the two most important parameters, its center and width. It is clear that the center and the standard width of the window function in Figure2.2 are 0 and 2τ , respectively. For a general window function $\phi(t)$, we define its center t^* as

$$t^* := \frac{1}{\|\phi\|^2} \int_{-\infty}^{\infty} t |\phi(t)|^2 dt \tag{2.10}$$

and the root-mean-square (RMS) radius Δ_ϕ as

$$\Delta_\phi := \frac{1}{\|\phi\|} \left[\int_{-\infty}^{\infty} (t-t^*)^2 |\phi(t)|^2 dt \right]^{1/2} \tag{2.11}$$

The function is called a time window. For the window of Figure2.2, use (2.10) and (2.11) to verify that $t^* = 0$ and $\Delta_\phi = \tau / \sqrt{3}$. Therefore, the RMS width is smaller than the standard width by a factor of $1/\sqrt{3}$.

From the function $\phi(t)$ described above, similarly, we can have a frequency window $\hat{\phi}(\omega)$ with center ω^* and the RMS radius $\Delta_{\hat{\phi}}$ defined analogous to (2.10) and (2.11) as

$$\omega^* := \frac{1}{\|\hat{\phi}\|^2} \int_{-\infty}^{\infty} \omega |\hat{\phi}(\omega)|^2 d\omega \tag{2.12}$$

$$\Delta_{\hat{\phi}} := \frac{1}{\|\hat{\phi}\|} \left[\int_{-\infty}^{\infty} (\omega - \omega^*)^2 |\hat{\phi}(\omega)|^2 d\omega \right]^{\frac{1}{2}} \tag{2.13}$$

Theoretically, A function cannot be limited in time and frequency simultaneously. Verifying $\phi(t)$ for the window of Figure2.2, $\omega^* = 0$ and $\Delta_{\phi} = \infty$, this window is the best time window but the worst frequency window.

2.2.2　Short-time Fourier transform

We want to obtain the properties of a signal $f(t)$ in the neighborhood of some desired location in time $t = b$, by multiplying an appropriated window function $\phi(t)$ to produce the windowed function $f_b(t) = f(t)\phi(t-b)$ and then taking the Fourier transform of $f_b(t)$. This is the short-time Fourier transform (STFT). Formally, we can define the STFT of a function $f(t)$ with the window function $\phi(t)$ discussed in Section 2.2.1 in the time-frequency plane as

$$G_{\phi} f(b,\xi) := \int_{-\infty}^{\infty} f(t) \overline{\phi_{b,\xi}(t)} dt \tag{2.14}$$

where

$$\phi_{b,\xi}(t) := \phi(t-b) e^{j\xi t} \tag{2.15}$$

Because of the windowing nature of the STFT, this transform is referred to as the windowed Fourier transform.

2.2.3 Time-Frequency Window

Let us consider the window function $\phi(t)$ in (2.15). If t^* is the center and Δ_ϕ the radius of the window function, then (2.14) gives the information of the function $f(t)$ in the time window:

$$[t^* + b - \Delta_\phi, t^* + b + \Delta_\phi] \tag{2.16}$$

To derive the corresponding window in frequency domain, apply Parseval's identity to (2.14). We have

$$G_\phi f(b,\xi) := \int_{-\infty}^{\infty} f(t)\overline{\phi(t-b)}e^{-j\xi t}dt \tag{2.17}$$

$$= \frac{1}{2\pi}e^{-j\xi b}\int_{-\infty}^{\infty} \hat{f}(\omega)\overline{\hat{\phi}(\omega-\xi)}e^{-jb\omega}d\omega$$

$$= e^{-j\xi b}\left[\hat{f}(\omega)\overline{\hat{\phi}(\omega-\xi)}\right]^{\vee}(b) \tag{2.18}$$

where the symbol "$\vee$" represents the inverse Fourier transform. Observe that (2.17) has a form similar to (2.14). If ω^* is the center and $\Delta\hat{\phi}$ is the radius of the window function $\hat{\phi}(\omega)$, then (2.17) gives us information about the function $\hat{f}(\omega)$ in the interval

$$[\omega^* + \xi - \Delta\hat{\phi}, \omega^* + \xi + \Delta\hat{\phi}] \tag{2.19}$$

Because of the similarity of representation in (2.14) and (2.17), the STFT give information about the function $f(t)$ in the time-frequency widow:

$$[t^* + b - \Delta_\phi, t^* + b + \Delta_\phi] \times [\omega^* + \xi - \Delta\hat{\phi}, \omega^* + \xi + \Delta\hat{\phi}] \tag{2.20}$$

Figure 2.3 represents graphically the notion of the time-frequency windowgiven by (2.19). Here we have assumed that $t^* = \omega^* = 0$.
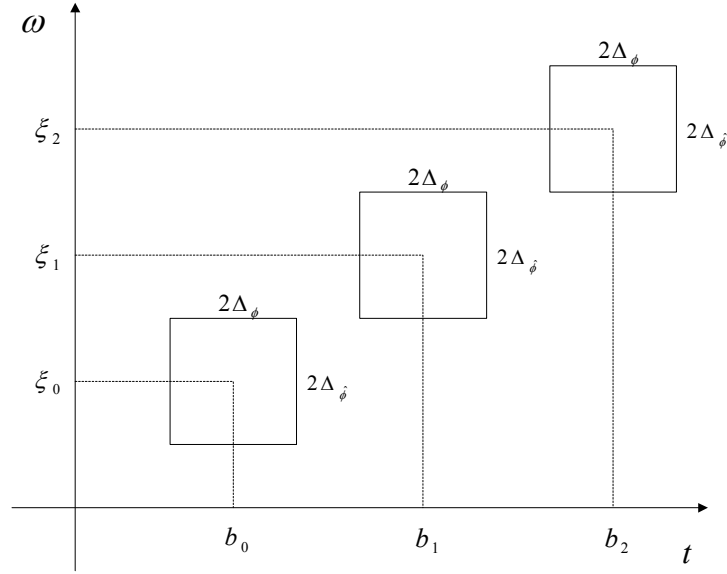
Figure 2.3: Time-frequency window for short-time Fourier transform($t^* = \omega^* = 0$)

2.3 Variable Structure Control

The Variable Structure Control(VSC) have the advantages of faster response and smaller sensitivity to system uncertainties and disturbances. In this thesis, we will adopt VSC schemes to design our controller. In this section we review some basic concept of VSC theory first.

2.3.1 Sliding Surface

Consider a single-input dynamic system

$$x^{(n)} = f(x) + b(x)u \tag{2.21}$$

where the scalar x is the output of interest, the scalar u is the control input, and $X = [x \quad \dot{x} \quad \dots \quad x^{(n-1)}]^T$ is the state vector. In system (2.21), the functions $f(x)$ and $b(x)$ (in general, nonlinear) are not exactly known, but the extent of the imprecision on $f(x)$ is upper bounded by a known continuous function of x, and control gain $b(x)$ is of known sign and bounded by a known continuous function of x, respectively. For example, the inertia of a mechanical system is only known to a certain accuracy, and friction models only describe part of the actual friction forces.

1 2

The control problem is to get the state x to track a specific time-varying state $X_d = [x_d \quad \dot{x}_d \quad \ldots \quad x_d^{(n-1)}]^T$ in the presence of model uncertainty on $f(x)$ and $b(x)$.

For the tracking task by using a finite control u, the initial desired state $x_d(0)$ must be such that :

$$x_d(0) = x(0) \qquad (2.22)$$

In a second-order system, for example, position or velocity can not "jump", so that any desire trajectory feasible from $t = 0$ necessarily starts with the same position and velocity as those of the plant. Otherwise, tracking can only be achieved after a transient.

Define $\tilde{x} = x - x_d$ is the tracking error in the variable x, and let

$$\tilde{x} = x - x_d = [\tilde{x} \quad \dot{\tilde{x}} \quad \ldots \quad \tilde{x}^{(n-1)}]^T$$

to be the tracking error vector. Furthermore, let us define a time-varying surface $S(t)$ in the state-space $R^{(n)}$ by the scalar equation $s(X;t) = 0$, where

$$s(X;t) = (\frac{d}{dt} + \lambda)^{n-1} \tilde{x} \qquad (2.23)$$

Given initial condition (2.22), the tracking problem $X \equiv X_d$ is equivalent to that of remaining on the surface $S(t)$ for all $t > 0$; indeed $s \equiv 0$ represents a linear differential equation whose unique solution is $\tilde{x} \equiv 0$, given initial conditions (2.22). Thus, the problem of tracking the n-dimensional vector x_d can be reduced to that of keeping the scalar portion s at zero. More precisely, the problem of tracking the n-dimensional vector x_d can in effect be replaced by a $1^{st} - order$ stabilization problem in s. Indeed, since from (2.23) the expression of s contains $\tilde{x}^{(n-1)}$, we only need to differentiate s once for the input u to appear. Furthermore, bounds on s can be directly translated into bounds on the tracking error vector $\tilde{x}$, and

therefore the scalar s represents a true measure of tracking performance. Then, $1^{st} - order$ problem of keeping the scalar s at zero can be achieved by choosing the control law u of the system (2.21) such that outside of $S(t)$

$$\frac{1}{2}\frac{d}{dt}s^2 \leq -\eta|s| \tag{2.24}$$

where η is a strictly positive constant. Practically, (2.24) states that the squared "distance" to the surface, as measured by s^2, decrease along system trajectory. Thus, it constrains trajectories to points towards the surface $S(t)$, as illustrated in Figure 2.4. In particular, once on the surface, the system trajectories remain on the the surface. In other words, satisfying sliding condition (2.24), makes the surface an invariant set. Furthermore, as we shall see, (2.24) also implies that some disturbances or dynamics uncertainties can be tolerated while still keeping the surface an invariant set. Graphically, this corresponds to the fact that in Figure 2.4 the trajectories off the surface can "move" while still pointing towards the surface. $S(t)$ verifying (2.24) is referred to as a <u>sliding surface</u>, and the system's behavior once on the surface is called <u>sliding mode</u>.
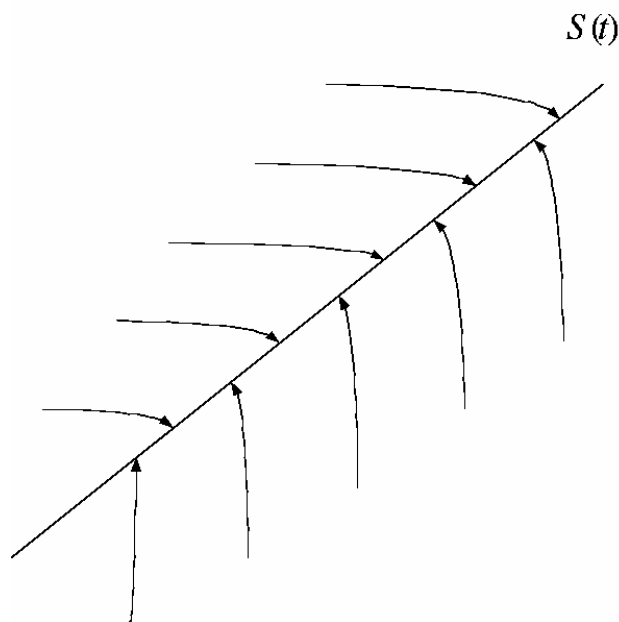
Figure 2.4: The sliding condition

The other interesting appearance of the invariant set $S(t)$ is that once on it, the system trajectories are defined by the equation of the set itself, namely

$$(\frac{d}{dt} + \lambda)^{n-1} \widetilde{x} = 0$$

In other words, the surface $S(t)$ is both a place and a dynamics. This fact is simply the geometric interpretation of the definition (2.23) allow us, in effect, to replace an $n^{th} - order$ problem by a $1^{st} - order$ one. Finally, satisfying (2.24) guarantees that if condition (2.22) is not exactly verified, ie., if $X(t = 0)$ is actually off $X_d(t = 0)$, the surface $S(t)$ will yet be reached in a finite time smaller than $|s(t = 0)|/\eta$. Indeed, assume for instance that $s(t = 0) > 0$, and let t_{reach} be the time required to hit the surface $s = 0$. Integrating (2.24) between $t = 0$ and $t = t_{reach}$ leads to

$$0 - s(t = 0) = s(t = t_{reach}) - s(t = 0) \leq -\eta(t_{reach} - 0)$$

while implies that

$$t_{reach} \leq s(t = 0)/\eta$$

Furthermore, definition (2.23) implies that once on the surface, the tracking error tends exponentially to zero, with a time constant $(n-1)/\lambda$ (form the sequence of $(n-1)$ filters of time constants equal to $1/\lambda$.

The typical system behavior implied by satisfying sliding condition (2.24) is illustrated in Figure 2.5 for $n = 2$. The sliding surface is a line in the phase plane, of slope $-\lambda$ and containing the (time-varying) point $X_d = [X_d \quad \dot{X}_d]^T$. Starting from any initial condition, the state trajectory reaches the time-varying surface in a finite time smaller than $s(t = 0)/\eta$, and then slide along the surface towards X_d exponentially, with a time-constant equal to $1/\lambda$.

15
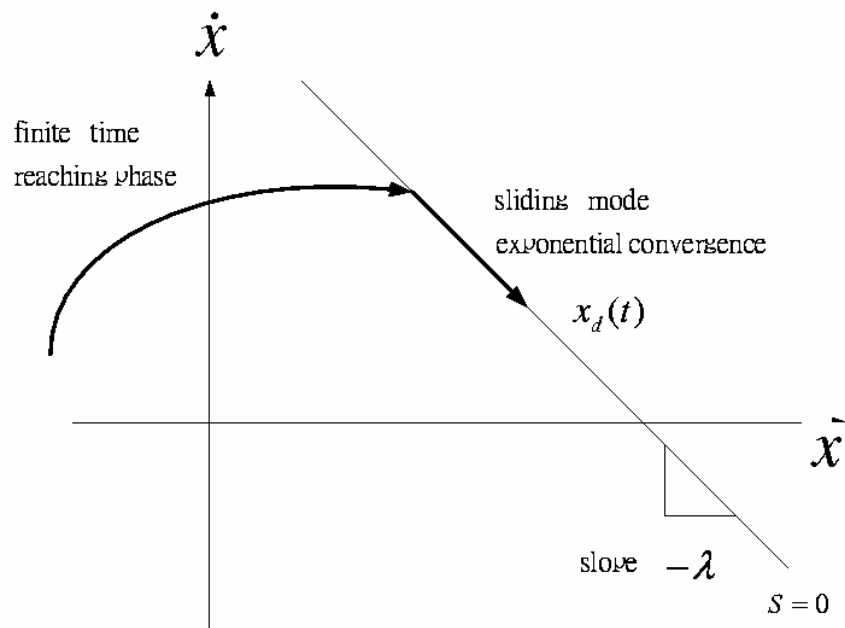
Figure 2.5: Graphical interpretation of equations (2.23) and (2.24) ($n = 2$)

In summary, the idea behind equations (2.23) and (2.24) is to choose a well-behaved function of the tracking error, s, according to (2.23), and then select the feedback control law u in system (2.21) such that s^2 remains a Lyapunov-like function of the closed-loop system, despite the presence of model uncertainties and disturbances. The controller design procedure then consists of two steps. First, a feedback control law u is selected so as to verifying sliding condition. However, in order to account for the presence of modeling uncertainties and disturbances, the control law has to be discontinuous across $S(t)$. Since the implementation of the associate control switchings is necessarily imperfect (for example, in practice switching is not instantaneous, and the value s is not known with infinite precision), this leads to chattering as showing in Figure 2.6.

1 6
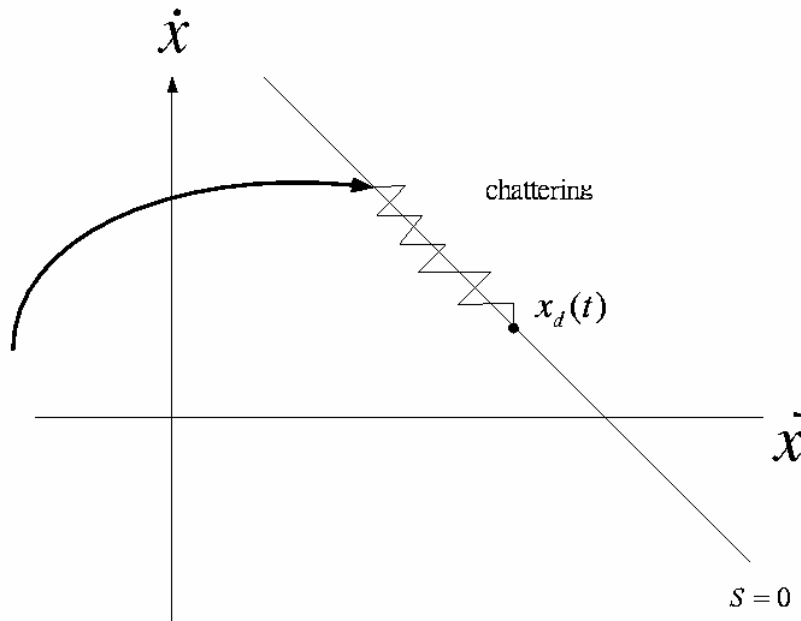
Figure 2.6 Chattering as result of imperfect control switching

The chattering is undesirable in practice, since it involves high control activity and further may excite high-frequency dynamics neglected in the course of modeling (such as unmodeled structure modes, neglected time-delays, and so on). Thus, in a second step, the discontinuous control law u is suitably smoothed to achieve an optimal trade-off between control bandwidth and tracking precision: while the first step accounts for parametric uncertainty, the second step achieves robustness to high-frequency unmodeled dynamics.

2.3.2 Variable Structure Control Design

The implementation of the Variable Structure Control (VSC) consists of two main phases. First, we should construct the sliding surface such that the system states restricted to the sliding surface will produce the desired behavior. Second, we construct switched feedback gain which derive the plant state trajectory to the sliding surface in finite time and restrict the state to sliding surface. The method of equivalent control is means of determining the system motion restricted to the sliding surface.

Suppose at t_0, the state trajectory of the plant intercepts the sliding surface and a sliding mode exists for all $t > t_0$. The existence of a sliding mode implies (1) $\dot{s} = 0$, and (2) $s = 0$ for all $t > t_0$. The system's motions on the sliding surface can be given an interesting geometric interpretation, as an "average" of the systems' dynamics on both sides of the surface. The system while in sliding mode can be written as

$$\dot{s} = 0 \tag{2.25}$$

By solving the above equation formally for the control input, we obtain an expression for u called the <u>equivalent control</u>, u^{eq} which can be interpreted as the continuous control law that would maintain $\dot{s} = 0$ if the dynamics were exactly known. For example, for a second-order system

$$\ddot{x} = f + u \tag{2.26}$$

In order to have the system track $x(t) = x_d(t)$, we define a sliding surface $s = 0$ according to (2.23), namely:

$$s = (\frac{d}{dt} + \lambda)\tilde{x} = \dot{\tilde{x}} + \lambda\tilde{x} \tag{2.27}$$

We then have:

$$\dot{s} = \ddot{x} - \ddot{x}_d + \lambda\dot{\tilde{x}} = f + u - \ddot{x}_d + \lambda\dot{\tilde{x}} \tag{2.28}$$

the equivalent control u^{eq} of a continuous control law that would achieve $\dot{s} = 0$ is

$$u^{eq} = -f + \ddot{x}_d - \lambda\dot{\tilde{x}} \tag{2.29}$$

and the system dynamics while in sliding mode is

$$\ddot{x} = f + u^{eq} = \ddot{x}_d - \lambda\dot{\tilde{x}} \tag{2.30}$$

Geometrically, the equivalent control can be constructed as

$$u^{eq} = \alpha u^+ + (1 - \alpha)u^- \tag{2.31}$$

i.e., as a convex combination of the value of u on both sides of the surface $S(t)$. The value of α can again be obtained formally from (2.25), which corresponds to

requiring the system trajectories be tangent to the surface. This intuitive construction is summarized in Figure 2.7, where $f^+ = [\dot{x} \quad f + u^+]^T$, and similarly $f^- = [\dot{x} \quad f + u^-]^T$ and $f^{eq} = [\dot{x} \quad f + u^{eq}]^T$. Its formal justification was derived in the early 1960's by the Russian mathematician A.F.Filippov.
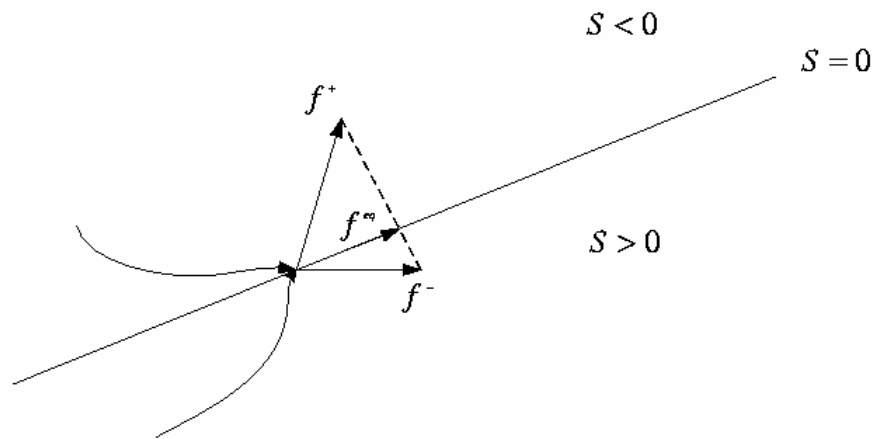
Figure 2.7: Filippov's construction of the equivalent dynamics in sliding mode

Controller design is the second phase of the VSC design procedure. Here the goal is to determine switched feedback gains which derive the plant state trajectory to the sliding surface and maintain a sliding mode condition. The presumption is that the sliding surface has been designed. Among several approach (e.g. the diagonalization method and hierarchical control method), augmenting the equivalent control is one popular approach. This structure of control of system (2.26) is

$$u = u^{eq} + u^{re} \qquad (2.32)$$

where u^{re} is the discontinuous or the switched part of (2.32). Consider the system (2.26), we have $u^{eq} = -f + \ddot{x}_d - \lambda\dot{\tilde{x}}$. In order to satisfy sliding condition (2.24), we add to u^{re} a term discontinuous across the surface $s = 0$, and let

$$
\begin{aligned}
u &= u^{eq} + u^{re} \\
&= u^{eq} - k\,\mathrm{sgn}(s)
\end{aligned}
\qquad (2.33)
$$

where sgn is the sign function

$$\text{sgn}(s) = \begin{cases} 1 & if \quad s > 0 \\ 0 & if \quad s = 0 \\ -1 & if \quad s < 0 \end{cases} \tag{2.34}$$

By selecting k to be a positive scalar, then

$$\frac{1}{2}\frac{d}{dt}s^2 = \dot{s} \cdot s = -k\,\text{sgn}(s) \cdot s = -k|s| \le -\eta|s|$$

For k is large enough, we can guarantee that (2.24) is verified.

2.4 Adaptive Control

Many dynamic systems to be controlled have constant or slowly-varying uncertain parameters. For instance, Power systems may be subjected to large variations in loading conditions. Adaptive control is an approach to the control of such system. The basic idea in adaptive control is to estimate the uncertain plant parameters (or, equivalently, the corresponding controller parameters) on-line based on the measured system signal, and use the estimated parameters in the control input computation. An adaptive control system can thus be regarded as a control system with on-line parameter estimation.

An adaptive controller differs from an ordinary controller in that the controller parameters are variable, and there is a mechanism for adjusting these parameters on-line based on signals in the system. There are two main approaches for constructing adaptive controllers. One is the so-called model-reference adaptive control method, and the other is the so-called self-tuning method.

Model-reference adaptive control (MRAC)

Generally, a model-reference adaptive control system can be schematically represented by Figure 2.8. It is composed of four parts: a plant containing unknown parameters, a reference model for compactly specifying the desired output of the control system, a feedback control law containing adjustable parameters, and an adaptation mechanism for updating the adjustable parameters.

$\hat{a}$ --- estimated parameters
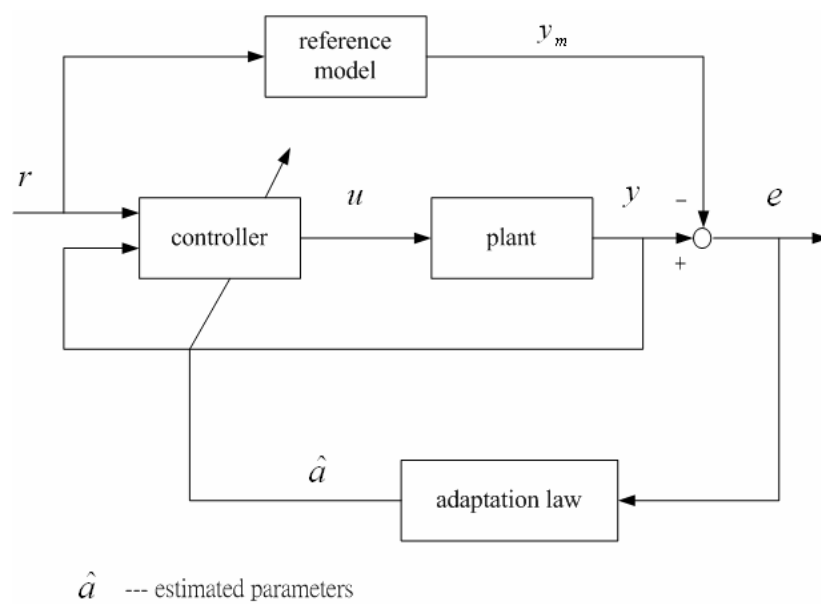
Figure 2.8 A model-reference adaptive control system

The plant is assumed to have a known structure, although the parameters are unknown, for linear plants, this means that the number of poles and the number of zeros are assumed to be known, but that the locations of these poles and zeros are not. For nonlinear plants, this implies that the structure of the dynamic equations is known, but that some parameters are not.

A reference model is used to specify the ideal response of the adaptive control system to the external command. Intuitively, it provides the ideal plant response which the adaptation mechanism should seek in adjusting the parameters. The choice

of the reference model is part of the adaptive control system design. This choice has to satisfy two requirements. On the one hand, it should reflect the performance specification in the control tasks, such as rise time, settling time, overshoot or frequency domain characteristics. On the other hand, this ideal behavior should be achievable for the adaptive control system, i.e., there are some inherent constraints on the structure of the reference model (e.g., its order and relative degree) given the assumed structure of the plant model.

The controller is usually parameterized by a number of adjustable parameters (implying that one may obtain a family of controllers by assigning various values to the adjustable parameters). The controller should have perfect tracking capacity in order to allow the possibility of tracking convergence. That is, when the plant parameters are exactly known, the corresponding controller parameters should make the plant output identical to that of the reference model. When the plant parameters are not known, the adaptation mechanism will adjust the controller parameters so that perfect tracking is asymptotically achieved. If the control law is linear in terms of the adjustable parameters, it is said to be linearly parameterized. Existing adaptive control designs normally require linear parametrization of the controller in order to obtain adaptation mechanisms with guaranteed stability and tracking convergence.

The adaptation mechanism is used to adjust the parameters in the control law. In MRAC systems, the adaptation law searches for parameters such that the response of the plant under adaptive control becomes the same as that of the reference model, i.e., the objective of the adaptation is to make the tracking error converge to zero. Clearly, the main difference from conventional control lies in the existence of this mechanism. The main issue in adaptation design is to synthesize an adaptation mechanism which will guarantee that the control system remains stable and the tracking error converges to zero as the parameters are varied. Many formalisms in nonlinear control can be

used to this end, such as Lyapunov theory, hyperstability theory, and passivity theory. Although the application of one formalism may be more convenient than that of another, the results are often equivalent.

Self-tuning controllers (STC)

In non-adaptive control design (e.g., pole placement), one computes the parameters of the controllers from those of the plant. If the plant parameters are not known, it is intuitively reasonable to replace them by their estimated values, as provided by a parameter estimator. A controller thus obtained by coupling a controller with an on-line (recursive) parameter estimator is called a self-tuning controller. Figure 2.9 illustrates the schematic structure of such an adaptive controller. Thus, a self-tuning controller is a controller which performs simultaneous identification of the unknown plant.

$\hat{a}$ --- estimated parameters
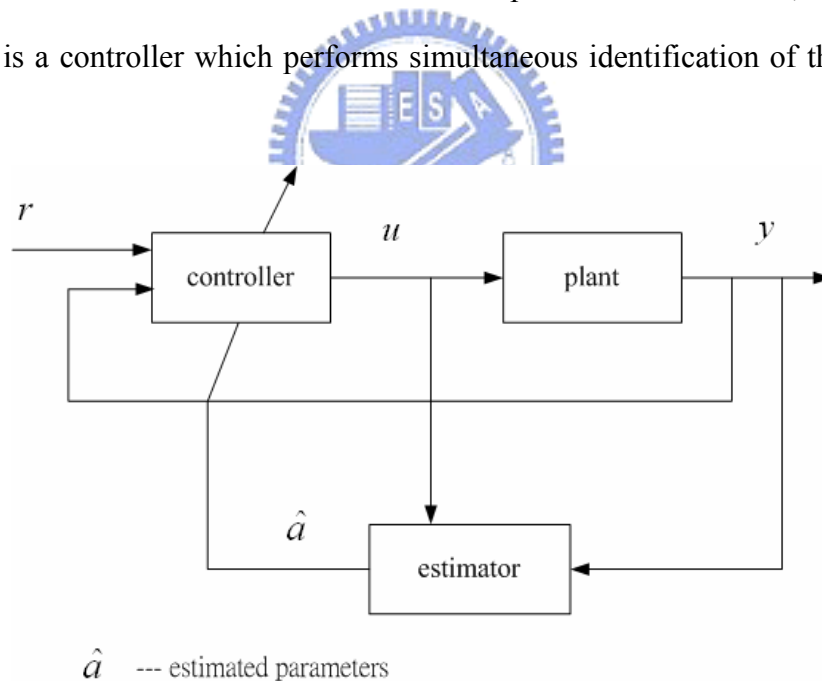
Figure 2.9 A self-tuning controller

The operation of a self-tuning controller is as follows: at each time instant, the estimator sends to the controller a set of estimated plant parameters, which is computed based on the past plant input u and output y; the computer finds the corresponding controller parameters, and then computes a control input u based on

2 3

the controller parameters and measured signals; this control input u causes a new plant output to be generated, and the whole cycle of parameter and input updates is repeated. Note that the controller parameters are computed from the estimates of the plant parameters as if they were the true plant parameters. This idea is often called the certainty equivalence principle.

Parameter estimation can be understood simply as the process of finding a set of parameters that fits the available input-output data from a plant. This is different from parameter adaptation in MRAC systems, where the parameters are adjusted so that the tracking errors converge to zero. For linear plants, many techniques are available to estimate the unknown parameters of the plant. The most popular one is the least-squares method and its extensions. There are also many control techniques for linear plants, such as pole-placement, PID, LQR (linear quadratic control), minimum variance control, or H^∞ designs. By coupling different control and estimation schemes, one can obtain a variety of self-tuning regulators. The self-tuning method can also be applied to some nonlinear systems without any conceptual difference.

In the basic approach to self-tuning control, one estimates the plant parameters and then computes the controller parameters. Such a scheme is often called indirect adaptive control, because of the need to translate the estimated parameters into controller parameters. It is possible to eliminate this part of the computation. to do this, one notes that the control law parameters and plant parameters are related to each other for a specific control method. This implies that we may reparameterize the plant model using controller parameters (which are also unknown, of course), and then use standard estimation techniques on such a model. Since no translation is needed in this scheme, it is called a direct adaptive control scheme. In MARC systems, one can similarly consider direct and indirect ways of updating the controller parameters.

CHAPTER 3

Detection of Voltage Collapse for the Electric Power Systems

In this chapter, we first introduce the dynamical equations of electric power systems that proposed by Dobson and Chiang [9]. Then, we apply the FIDF and signal analysis tool to the detection of voltage collapse in a power system.

3.1 Dynamical Equations of Electric Power Systems

It is known that load characteristic has a significant effect on a power system dynamics [6,35]. Therefore the voltage collapse cannot be studied using classical models, such as constant PQ, constant impedance, and constant current models, which

assume the magnitude of the load voltage to be constant. In this thesis, we adopt the power system model from Dobson and Chiang [9] as below:

The Load Model: The nonlinear load model (3.1)-(3.2) below is originally introduced by Walve [31] and then modified by [9]. It includes a dynamic induction motor model with a constant PQ load. The combined model for the motor and the PQ load has the following form:

$$P = P_0 + P_1 + K_{pw}\dot{\delta} + K_{pv} + \left(V + T\dot{V}\right) \tag{3.1}$$

$$Q = Q_0 + Q_1 + K_{qw}\dot{\delta} + K_{qv}V + K_{qv2}V^2 \tag{3.2}$$

where P_0 and Q_0 are the constant real and reactive powers of the motor, P_1 and Q_1 represent the PQ load, and the remaining parameters are same as those given in [9].
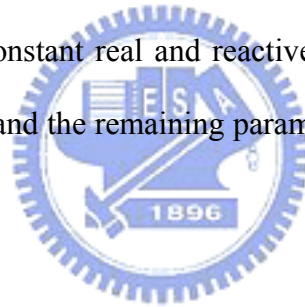
The Power System Model: The power system model in this thesis is adopted from Dobson and Chiang [9] as shown in Figure 3.1.(a). In this model, one generator is a slack bus while the other has constant voltage magnitude E_m and angle δ_m satisfies the following swing equation:

$$M\ddot{\delta}_m = -d_m\omega + P_m + E_m V Y_m \sin\left(\delta - \delta_m - \theta_m\right) + E_m^2 Y_m \sin\theta_m \tag{3.3}$$

where M, d_m and P_m denote the generator inertia, damping and mechanical power, respectively. In the model, Q_1 is chosen as the system parameter so that increasing Q_1 corresponds to increasing the load reactive power demand. In addition, the load also includes a fixed capacitor C to raise the voltage up to near 1.0 per unit.

2 6

To facilitate the analysis, it is convenient to account for the capacitor by adjusting E_0 and Y_0 to give the Th'evenin equivalent of the circuit with the capacitor. The adjusted values are

$$E_0' = E_0 / \left(1 + C^2 Y_0^{-2} - 2CY_0^{-1} \cos\theta_0\right)^{1/2} \tag{3.4}$$

$$Y_0' = Y_0 \left(1 + C^2 Y_0^{-2} - 2CY_0^{-1} \cos\theta_0\right)^{1/2} \tag{3.5}$$

$$\theta_0' = \theta_0 + \tan^{-1} \left\{ \frac{CY_0^{-1}\sin\theta_0}{1 - CY_0^{-1}\cos\theta_0} \right\} \tag{3.6}$$

Obviously, the product $E_0'Y_0'$ and E_0Y_0 are being the same constant. Then we have the equivalent circuit as shown in Figure 3.1.(b).

(a)

(b)
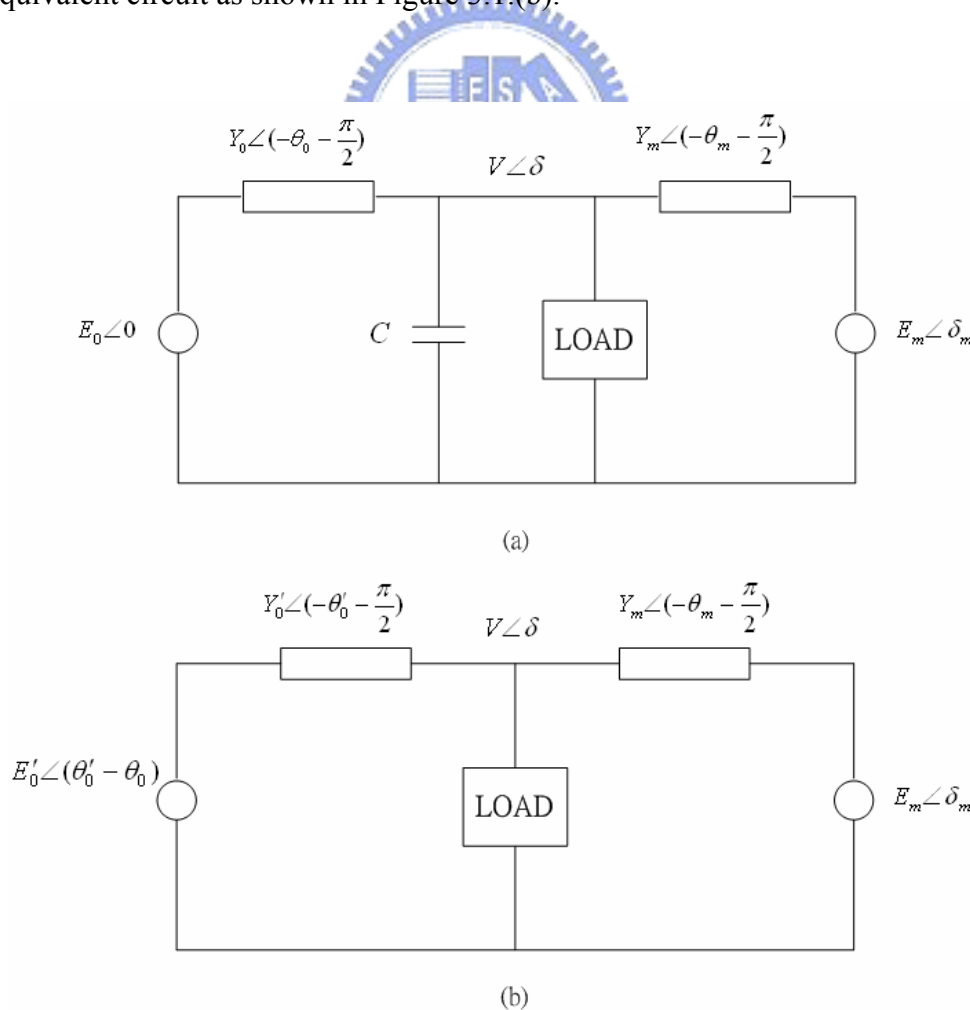
Figure 3.1: Power system model (a) original system (b) Th'evenin equivalent system

By calculating VI^* of the network, the real and reactive powers supplied by the network are

$$P = - E_0' Y_0' V \sin\left(\delta + \theta_0\right) - E_m Y_m V \sin\left(\delta - \delta_m + \theta_m\right)$$
$$+ \left(Y_0' \sin\theta_0' + Y_m \sin\theta_m\right) V^2 \tag{3.7}$$

$$Q = E_0' Y_0' V \cos\left(\delta + \theta_0\right) + E_m Y_m V \cos\left(\delta - \delta_m + \theta_m\right)$$
$$- \left(Y_0' \cos\theta_0' + Y_m \cos\theta_m\right) V^2 \tag{3.8}$$

From Eqs. (3.3) and equating (3.1)-(3.2) with (3.7)-(3.8), we have the overall dynamical equations for the electric power system as below:

$$\dot{\delta_m} = \omega \tag{3.9}$$

$$M\dot{\omega} = - d_m \omega + P_m + E_m Y_m V \sin\left(\delta - \delta_m - \theta_m\right)$$
$$+ E_m^2 Y_m \sin\theta_m \tag{3.10}$$

$$K_{qw}\dot{\delta} = - K_{qv2} V^2 - K_{qv} V + Q\left(\delta_m, \delta, V\right) - Q_0 - Q_1 \tag{3.11}$$

$$T K_{qw} K_{pv}\dot{V} = K_{pw} K_{qv2} V^2 + \left(K_{pw} K_{qv} - K_{qw} K_{pv}\right) V$$
$$+ K_{qw}\left(P(\delta_m, \delta, V) - P_0 - P_1\right)$$
$$- K_{pw}\left(Q(\delta_m, \delta, V) - Q_0 - Q_1\right) \tag{3.12}$$

where

$$Q(\delta_m, \delta, V) = E_0' Y_0' V \cos\left(\delta + \theta_0\right) + E_m Y_m V \cos\left(\delta - \delta_m + \theta_m\right)$$
$$- \left(Y_0' \cos\theta_0' + Y_m \cos\theta_m\right) V^2 \tag{3.13}$$

$$P(\delta_m, \delta, V) = - E_0' Y_0' V \sin\left(\delta + \theta_0\right) - E_m Y_m V \sin\left(\delta - \delta_m + \theta_m\right)$$
$$- \left(Y_0' \sin\theta_0' + Y_m \sin\theta_m\right) V^2 \tag{3.14}$$

In this thesis, the system parameters are adopted from [9] as follows:

The load parameters are

$K_{pw} = 0.4, K_{pv} = 0.3, K_{qw} = -0.03, K_{qv} = -2.8,$

$K_{qv2} = 2.1, T = 8.5, P_0 = 0.6, Q_0 = 1.3, P_1 = 0$

The network and generator parameters are

$Y_0 = 20.0, \theta_0 = -5.0, E_0 = 1.0, C = 12.0,$

$Y_0' = 8.0, \theta_0' = -12.0, E_0' = 2.5, Y_m = 5.0,$

$\theta_m = -5.0, E_m = 1.0, P_m = 1.0, d_m = 0.05, M = 0.3$

All parameters are in per unit expect for angles, which are in degrees.

Let $x_1 = \delta_m$, $x_2 = \omega$, $x_3 = \delta$, $x_4 = V$. Then Eqs. (3.9)-(3.12) can be written in the form of $\dot{x} = f(x, u)$, $u = Q_1$ as below:

$$\dot{x}_1 = x_2 \tag{3.13}$$

$$\dot{x}_2 = 3.33333\left(0.56422 - 0.05x_2 + \left(5x_4\sin\left(0.08727 - x_1 + x_3\right)\right)\right) \tag{3.14}$$

$$\dot{x}_3 = -33.33333\left(-1.3 - Q_1 + 2.8x_4 - 15.00486x_4^2\right.$$
$$\left. + 20x_4\cos\left(0.08727 - x_3\right) + \left(5x_4\cos\left(0.08727 + x_1 - x_3\right)\right)\right) \tag{3.15}$$

$$\dot{x}_4 = -13.0719\left(-1.111x_4 + 0.84x_4^2 - 0.4\left(-1.3 - Q_1 - 12.90486x_4^2\right.\right.$$
$$\left. + 20x_4\cos\left(0.08727 - x_3\right) + 5x_4\cos\left(0.08727 + x_1 - x_3\right)\right)$$
$$- 0.03\left(-0.6 - 2.17889x_4^2 + 20x_4\sin\left(0.08727 - x_3\right)\right.$$
$$\left.\left. + 5x_4\sin\left(0.08727 + x_1 - x_3\right)\right)\right) \tag{3.16}$$

The system equilibrium points can then be obtain by solving $f(x, Q_1) = 0$, which depends on the load reactive power parameter Q_1.

3.2 Voltage Collapse in the Electric Power Systems

The study of power system stability has attracted lots of attention (see e.g., [6,28,34] and the references therein). Among the possible instabilities, a serious type is the so-called "voltage collapse." This kind of instability in a power system is characterized by an initial slow progressive decline and then rapid decline in the voltage magnitude [17]. Two typical examples are shown in Figures 3.5(a) and 3.2(b). The voltage collapse behavior has been reported to be attributed to the increase of power demand that results in the operation of an electric power system near its stability limit [9,16,17]. As is well known, the qualitative change in the behavior of a nonlinear system with the change of one or more parameters is due to bifurcations. The variations of any parameter might result in complicated behavior and even give rise to system instabilities. Among the researches, for instance, Thomas and Tiranuchit [28] have pointed out that the induction motor dynamics could affect the voltage stability. Dobson and Chiang [8,9] have presented a mechanism for voltage collapse and introduced a simple power system model containing a generator, an infinite bus and a nonlinear load. They claimed that the voltage collapse behavior might occur around a saddle node bifurcation point. Abed et al. [1,2,32] have reported the oscillatory behavior of a power system using Hopf bifurcation theory.

3.3 Results of FIDF Design

In this section, the FIDF technique will be employed to detect the occurrence of voltage collapse in a power system described in Section 3.2. It is observed that, when system experiences a heavy load, the voltage might exhibit a growing oscillation and then sudden breakdown if the load exceeds a critical value, however, the scenario do not happen for it's linearized model. With this observation, a linear-based fault identification filter (FIDF) design technique is proposed to detect the voltage collapse. This is achieved by treating the difference between the output of the power system and that of its linearized model at a stable operating point as a fault vector and then investigating the effect of the fault on the designed FIDF.

In order to apply the FIDF results [5], we should construct the linearized model of the system (3.13)-(3.16) about an asymptotically stable operating point $x_0^T(Q_{10}) = (x_{10}, x_{20}, x_{30}, x_{40})^T$ for some given $Q_1 = Q_{10}$ as follows:

$$\dot{\hat{x}} = A\hat{x} + B\hat{Q}_1 \tag{3.17}$$

where $\hat{x} = x - x_0$ and $\hat{Q}_1 = Q_1 - Q_{10}$. Moreover, we assume that the available output of the power system has the form

$$y = C\hat{x} + D\hat{Q}_1, \tag{3.18}$$

where $C \in R^{p \times n}$ and $D \in R^{p \times m}$ are two constant matrices.

It is known that a linear model derived from a nonlinear one is a close approximation only near the operating point. To reduce the influence of the difference between the two models, it is suggested that the stable operating point for the power system be chosen to be close to the instability inception point. In this section the operating point is chosen to be close to the first Hopf bifurcation point.

Denote $y_{non}(t)$ and $y_{lin}(t)$ the output for nonlinear and linear model, respectively. It is noted that the two outputs $y_{non}(t)$ and $y_{lin}(t)$ are not equal in general. It is shown in [18] that the steady state output of the linearized model is linearly dependent on the input. We describe briefly as follow:

For the linearized model (3.17), (3.18), it is known that

$$y_{lin}(t) = Ce^{At}\hat{x}(0) + \int_0^t Ce^{A(t-\tau)}B\hat{Q}_1(\tau)d\tau + D\hat{Q}_1(t) \tag{3.19}$$

The first term on the right hand side of (3.19) depends only on the initial state while the second and third terms depend only on the input. Since the matrix A given in (3.17) is a Hurwitz matrix. It follows, $Ce^{At}\hat{x}(0) \to 0$ as $t \to \infty$. The input and output of the linearized model has the following relationship.

$$Y(s) = [C(sI - A)^{-1}B + D]Q(s) \tag{3.20}$$

where $Q(s)$ and $Y(s)$ are the Laplace transforms of $\hat{Q}_1(t)$ and $y_{lin}(t) - Ce^{At}\hat{x}(0)$, respectively. If the reactive power demand maintains a constant $\hat{Q}_1 = Q_{11}$. By Final Value Theorem and A is stable, we have

$$\lim_{t\to\infty} y_{lin}(t) - Ce^{At}\hat{x}(0)$$

$$= \lim_{s\to 0} sY(s)$$

$$= Q_{11}(-CA^{-1}B + D) \tag{3.21}$$

This means that the steady state output of the linearized model is linearly dependent on the input. However, when voltage collapse happens, the load voltage of the nonlinear model will exhibits a growing oscillatory voltage transient prior to voltage collapse. With these observations, the idea is to treat the difference $y_{non} - y_{lin}$ as a fault vector and then apply the FIDF technique to inspect the effect on this fault vector before voltage collapse occurs. In these simulations, we choose the load voltage V as the output which is easily measured. The output is then in the form

of (3.18) with

$$C = (0 \ 0 \ 0 \ 1) \quad \text{and} \quad D = 0 \tag{3.22}$$

for both the linear and nonlinear models.

It was shown from bifurcation analysis that the voltage collapse might occur when Q_1 is near the Hopf bifurcation point 10.89 [1,2,39]. This motivates us to choose the operating point at $Q_1 = 10.8$, which gives $x_0 = (0.1829, 0, -0.0068, 1.1031)^T$ as an equilibrium point. The matrix A given in (3.17) is found to be Hurwitz with eigenvalues $\{-133.73; -15.73; -0.01 \pm 3.76i\}$. Following the FIDF design procedure given in the Algorithm of section 2.1 with A and B given by (3.17), C and D given by (3.22), $E_1 = 0$ and $E_2 = 1$, the two filters $H_1(s)$ and $H_2(s)$ are designed to be

$$H_1(s) = \frac{-5.2288s^3 - 362.88s^2 - 157.51s - 5420.8}{(s+1)s^4 + 168.09s^3 + 2378.4s^2 + 2506.7s + 34043} \tag{3.23}$$

$$H_2(s) = \frac{1}{s+1} \tag{3.24}$$

The initial states are chosen as $(0.2, 0.2, 0.04, 0.98)^T$. The alarm signal is set to be 1 if |residual|>0.06 and equal to 0 elsewhere.

First, let the load reactive power demand be constant at 11.3 as in Figure 3.2(a). It is observed from Figure 3.2(b) that the load voltage collapse around $t = 1.13$. It means that the system undergoes voltage collapse for such heavy load. This is also recognizable from the change in the residual and alarm as displayed in Figure 3.2(c) and (d). The same scenario happens for small varying load as shown in Figure 3.3. Because the load in this case is smaller than that of Figure 3.2, the occurrence time of voltage collapse is clearly behind that of Figure 3.2. Next, a control effort to compensate reactive power is attempted in Figure 3.4 to recover from voltage collapse

when an alarm signal is detected. From Figure 3.4(b), the voltage collapse behavior disappears and the load voltage reaches an equilibrium point after a transient of oscillation. This can also be seen from Figure 3.4(c) and (d), where the alarm is turned off when the residual is less than the threshold value. This demonstrates that a proper control action can be applied to avoid the voltage collapse when such instabilities can be successfully detected. Finally, let us consider the situation about a 5% load variation. Figure 3.5 shows the simulation result of a 5% load variation about the operating point. It is observed from Figure 3.5(b) that the load voltage collapse around $t = 38$. By applying FIDF technique, the voltage collapse is successfully detected around $t = 34$ before it occurs. It provides us enough time to initiate appropriate control action to prevent such instability phenomena.

Figure 3.2: (a) load variation (Q_1) (b) load voltage

(c) residual signal   (d) alarm by FIDF

Figure 3.3: (a) load variation (Q_1) (b) load voltage

(c) residual signal   (d) alarm by FIDF
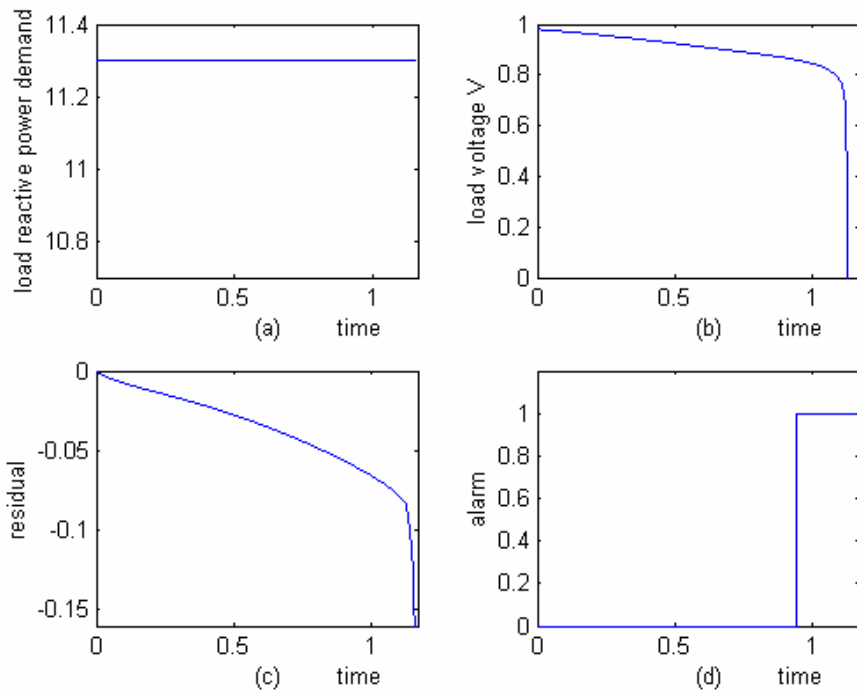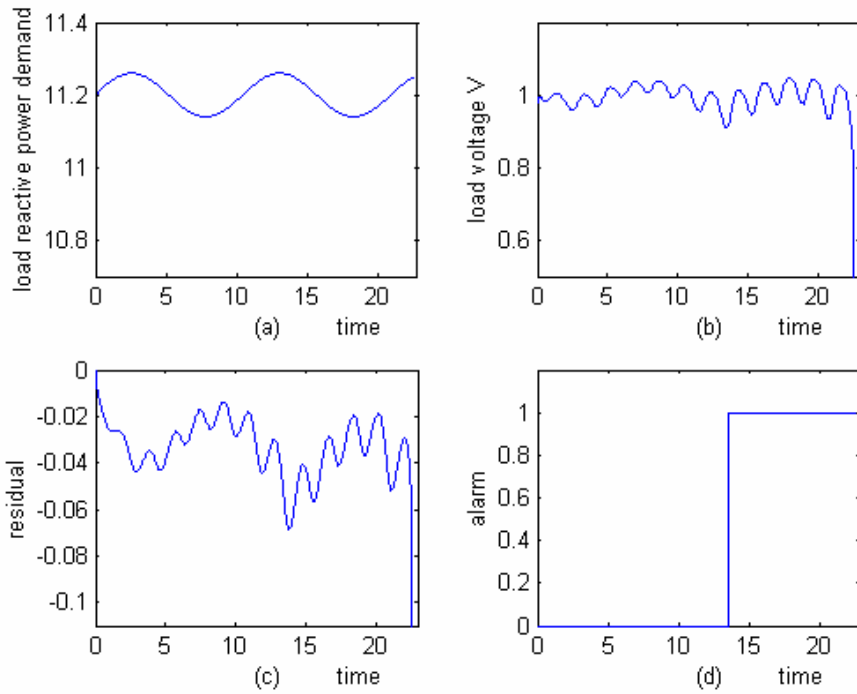
Figure 3.4: (a) load variation (Q_1) (b) load voltage

(c) residual signal (d) alarm by FIDF

Figure 3.5: (a) load variation (Q_1) (b) load voltage
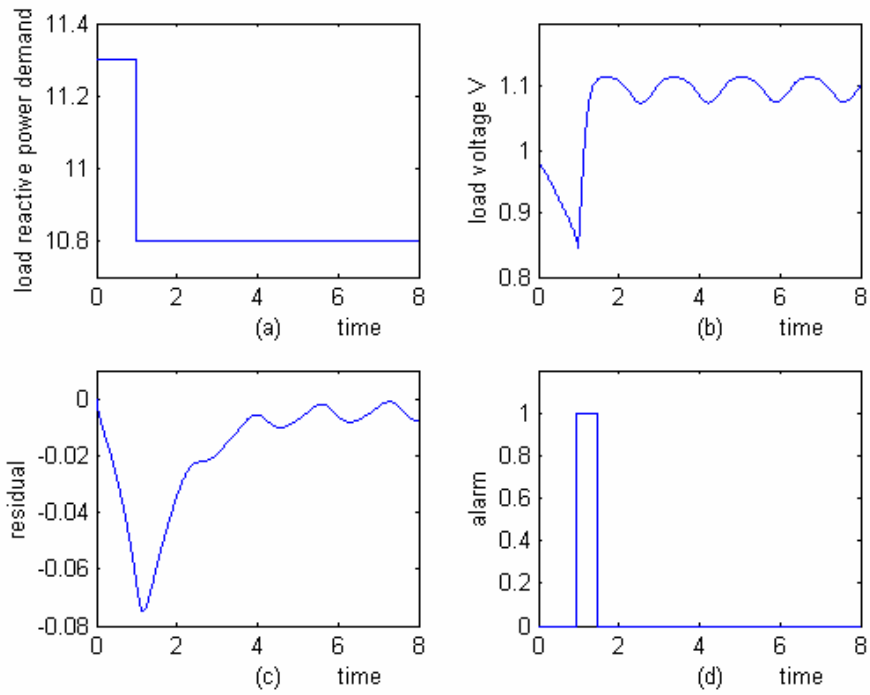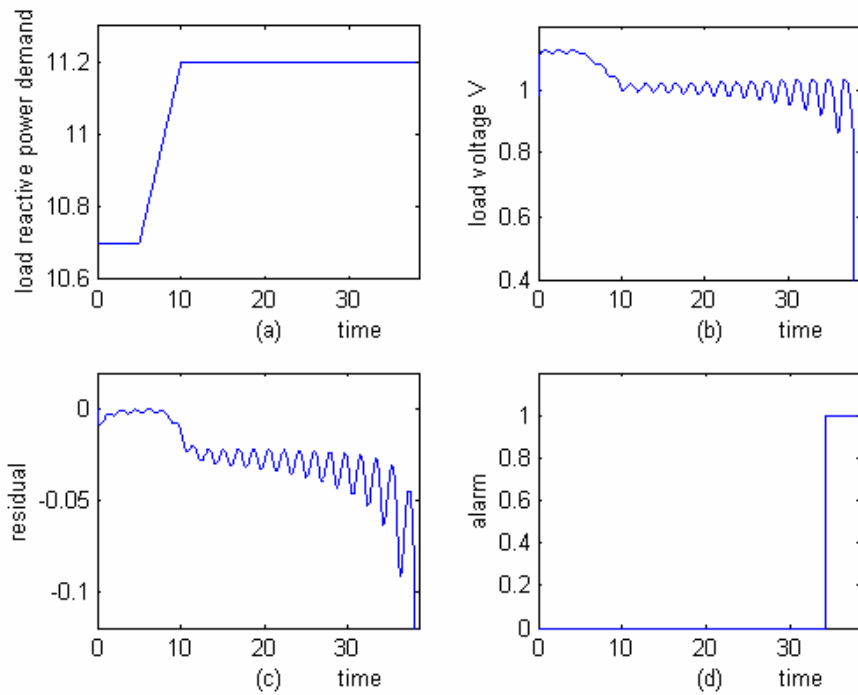
(c) residual signal (d) alarm by FIDF

3.4 Results of Signal Analysis

In addition to FIDF detection as discussed above, it is found from simulation that, when voltage collapse is about to happen for possible Q_1, the residual signals appear to exhibit oscillation with growing amplitude and almost the same frequency. As such, it enables us to monitor the amplitude of such a frequency to help judge the occurrence of voltage collapse. An example is shown in Figure 3.6, where the load voltage and residual signal for $Q_1 \equiv 11.1$ are given in Figures 3.6(a) and (b), respectively. To avoid the influence of DC part, an averaged signal from the residual by the formula (3.22) below

$$s_a(n) = s(n) - \frac{1}{L}\sum_{k=n-L+1}^{n} s(k), \quad L = 100 \tag{3.22}$$

and its spectrogram with sampling frequency $f_s = 100Hz$ are described in Figures 3.6(c) and (d), respectively. The oscillating frequency to be monitored is observed from Figure 3.6(d) to have $f \approx 0.59Hz$. The amplitude of the monitored frequency for the last 1024 points FFT before the occurrence of collapse versus Q_1 is shown by the solid-line of Figure 3.7. To facilitate the detection using the monitored frequency, the threshold values for different Q_1 are defined to be the amplitude of the monitored frequency 5 seconds ahead of voltage collapse, which are indicated by the dashed-line of Figure 3.7. Note that, the oscillating times before collapse are less than 5 seconds near the value of $Q_1 = 11.3$. With the definitions of threshold values, the voltage collapse for $Q_1 = 11.1$ is shown able to be successfully detected using both methods, as indicated in Figures 3.8(b) and (d). The alarm for the second method is fired around $t = 55$, which is near 5 seconds ahead of the collapse as desired. Finally, Figure 3.9 demonstrates the detection result for varying load using the threshold which is determined by the second method. Clearly, the alarm is also

fired nearly 5 seconds ahead of the occurrence of voltage collapse. Finally, we consider the situation of a 5% load variation about the operating point. Figure 3.10 shows the detection result. It is clear that the alarm is fired nearly 5 seconds ahead of the occurrence of voltage collapse as our desire.

From these simulations, it is noted that the voltage collapse can be successfully detected before it occurs. By properly adjusting the threshold for generating the alarm signal, the FIDF may provide a precursor of avoiding undesirable effects of these unstable behaviors.
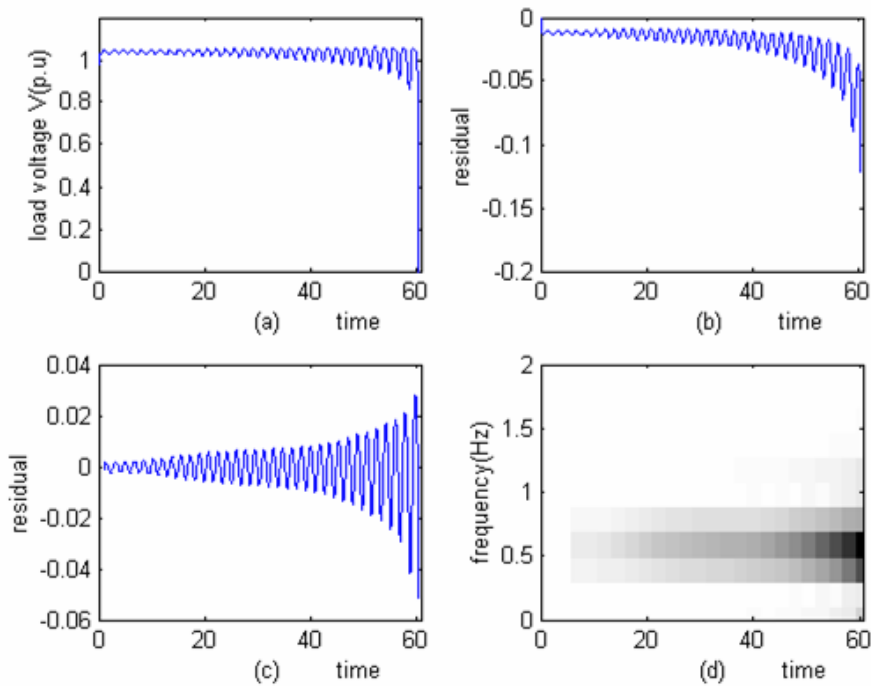
Figure 3.6: (a) Voltage response for $Q_1 \equiv 11.1$ (b) residual signal

(c) residual signal after averaging   (d) spectrogram
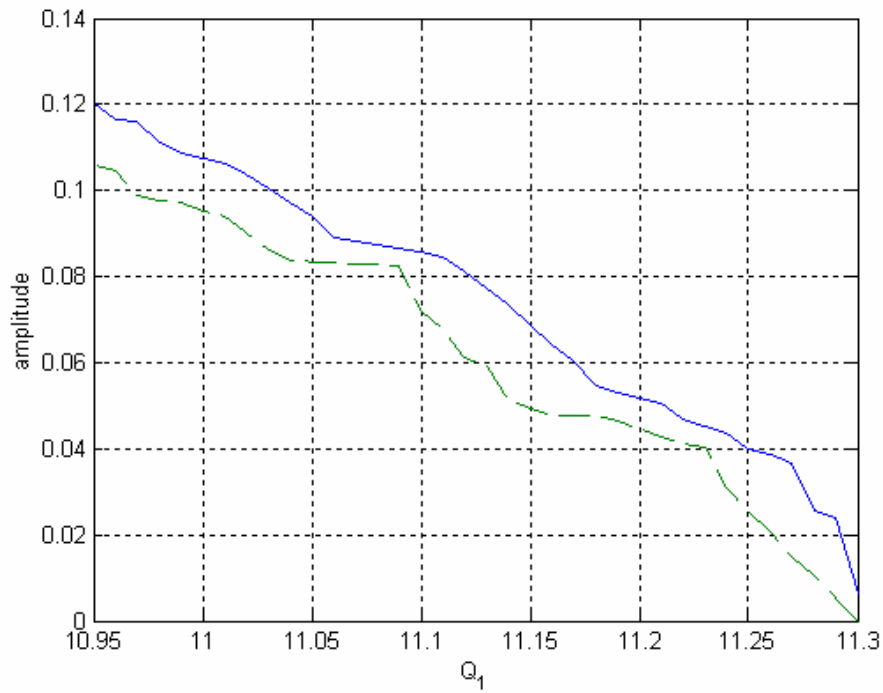
Figure 3.7: Amplitude of the monitored frequency versus Q_1
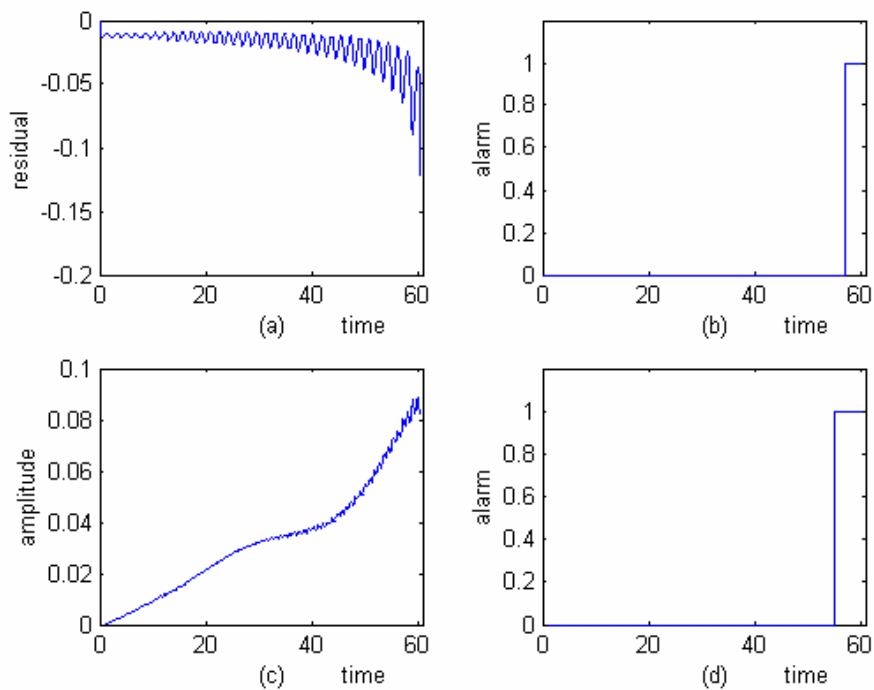
Figure 3.8: (a) residual signal for $Q_1 \equiv 11.1$ (b) alarm by FIDF (c) amplitude of

the monitored frequency (d) alarm by monitored frequency
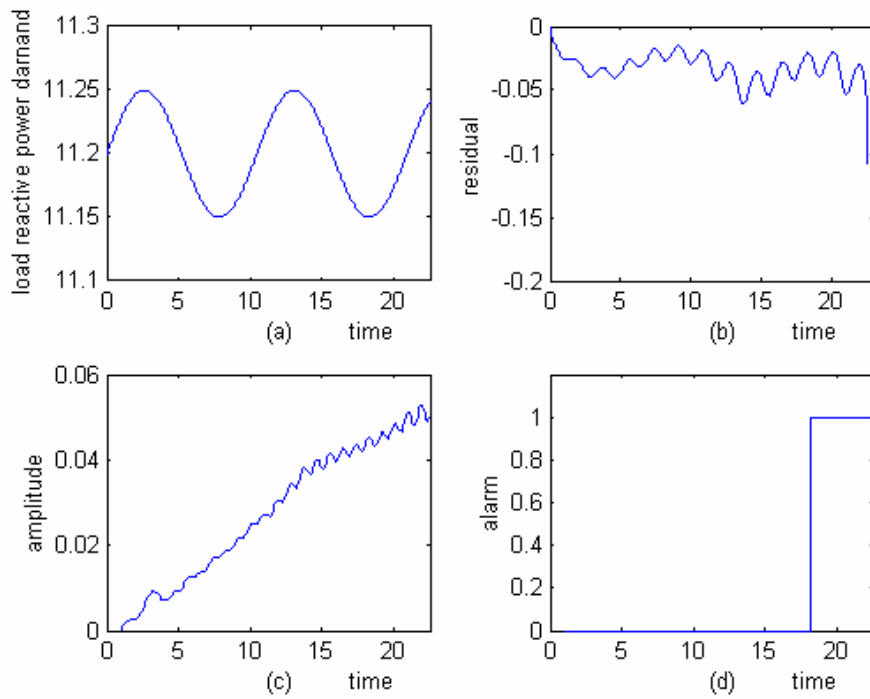
Figure 3.9: (a) load variation   (b) residual signal   (c) amplitude of the monitored

frequency   (d) alarm by monitored frequency
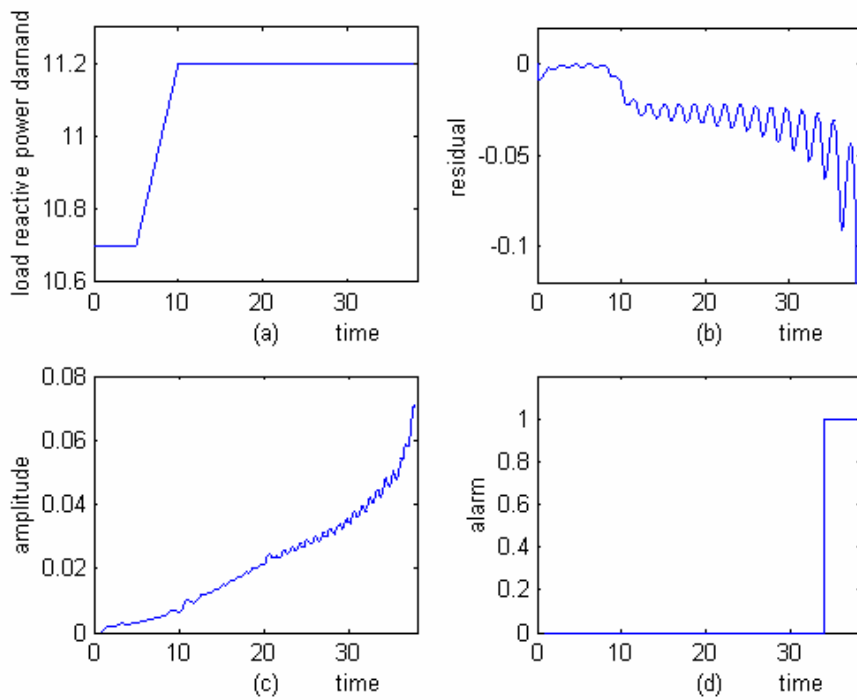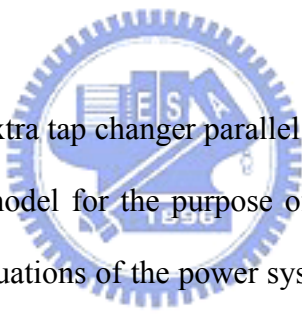
Figure 3.10: (a) load variation   (b) residual signal   (c) amplitude of the monitored

frequency   (d) alarm by monitored frequency

CHAPTER 4

Voltage Regulation of the Electric Power Systems

In this chapter, we add an extra tap changer parallel to the nonlinear load to Dobson and Chiang's power system model for the purpose of voltage regulation. In Section 4.1, we derive the dynamic equations of the power system with tap changer. Then, we will apply Variable Structure Control design scheme to adjust the tap changer ratio to achieve voltage regulation for this model. In Section 4.2, we propose a parameter estimator as the load monitor to provide the load variation of the power system. In Section 4.3, we combine the designs of VSC voltage controller and load estimator to design an adaptive control system.

4.1   Variable Structure Controller Design

4.1.1   Controlled Power System Model

In this section, we add a voltage controller – tap changer to the original power

system model. Here, we use the tap changer ratio as the control signal for the electric

power system. We will utilize tap changer to regulate the voltage of the electric power

system.

After adding a voltage controller – tap changer to the original power system model.

The controlled model is shown as in Figure 4.1.
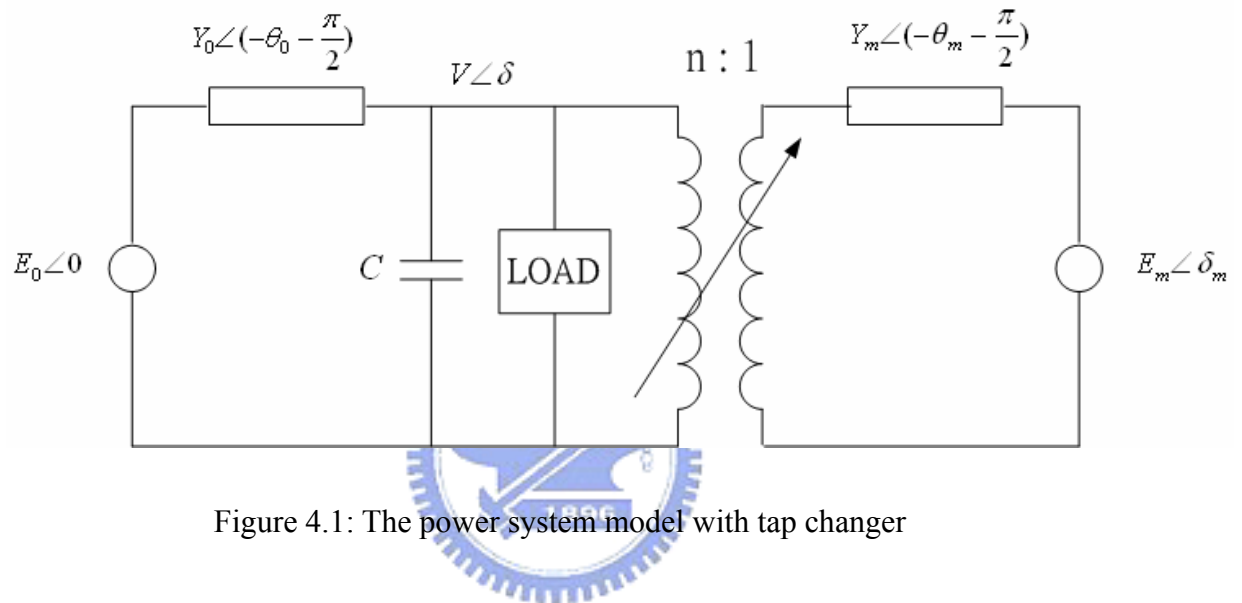
Figure 4.1: The power system model with tap changer

The original dynamical equations for the electric power system can be written as

follow :

$$\dot{\delta}_m = \omega \tag{4.1}$$

$$M\dot{\omega} = -d_m\omega + P_m + \frac{1}{n}E_mY_mV\sin\left(\delta - \delta_m - \theta_m\right)$$

$$+ E_m^2Y_m\sin\theta_m \tag{4.2}$$

$$K_{qw}\dot{\delta} = -K_{qv2}V^2 - K_{qv}V + Q\left(\delta_m, \delta, V\right) - Q_0 - Q_1 \tag{4.3}$$

$$TK_{qw}K_{pv}\dot{V} = K_{pw}K_{qv2}V^2 + \left(K_{pw}K_{qv} - K_{qw}K_{pv}\right)V$$

$$+ K_{qw}(P(\delta_m, \delta, V) - P_0 - P_1)$$

$$- K_{pw}(Q(\delta_m, \delta, V) - Q_0 - Q_1) \tag{4.4}$$

where

$$Q(\delta_m, \delta, V) = E_0'Y_0'V\cos(\delta + \theta_0) + \frac{1}{n}E_mY_mV\cos(\delta - \delta_m + \theta_m)$$

$$- \left(Y_0'\cos\theta_0' + \frac{1}{n^2}Y_m\cos\theta_m\right)V^2 \qquad (4.5)$$

$$P(\delta_m, \delta, V) = -E_0'Y_0'V\sin(\delta + \theta_0) - \frac{1}{n}E_mY_mV\sin(\delta - \delta_m + \theta_m)$$

$$- \left(Y_0'\sin\theta_0' + \frac{1}{n^2}Y_m\sin\theta_m\right)V^2 \qquad (4.6)$$

The system parameters we take are the same as those in the Section 3.1.

Let $x_1 = \delta_m$, $x_2 = \omega$, $x_3 = \delta$, $x_4 = V$. Then, Eqs. (4.1)-(4.4) can be written as :

$$\dot{x}_1 = x_2$$

$$\dot{x}_2 = 3.33333\left(0.56422 - 0.05x_2 + \left(5x_4n^{-1}\sin(0.08727 - x_1 + x_3)\right)\right)$$

$$\dot{x}_3 = -33.33333\left(-1.3 - Q_1 + 2.8x_4 - x_4^2(10.02389 + 4.98097n^{-2})\right.$$

$$\left. + 20x_4\cos(0.08727 - x_3) + \left(5x_4n^{-1}\cos(0.08727 + x_1 - x_3)\right)\right)$$

$$\dot{x}_4 = -13.0719\left(-1.111x_4 + 0.84x_4^2 - 0.4\left(-1.3 - Q_1 - x_4^2\left(7.92389\right.\right.\right.$$

$$\left. + 4.98097n^{-2}\right) + 20x_4\cos(0.08727 - x_3) + 5x_4n^{-1}\cos(0.08727$$

$$\left. + x_1 - x_3)\right) - 0.03\left(-0.6 + x_4^2(-1.74311 - 0.43578n^{-2})\right.$$

$$\left.\left. + 20x_4\sin(0.08727 - x_3) + 5x_4n^{-1}\sin(0.08727 + x_1 - x_3)\right)\right)$$

For convenience, we let $u = \frac{1}{n}$, and expand the above equations. Then the state equations become :

$$\dot{x}_1 = x_2 \tag{4.7}$$

$$\dot{x}_2 = 1.88073 - 0.16667x_2 + \left[16.66667x_4\sin(0.0827 - x_1 + x_3)\right]u \tag{4.8}$$

$$\dot{x}_3 = 43.33333 - 93.33333x_4 + 334.12967x_4^2 - 666.66667x_4\cos(0.08727$$
$$- x_3) + 33.33333Q_1 - \left[166.66667x_4\cos(0.08727 + x_1 - x_3)\right]u$$
$$+ 166.03245x_4^2u^2 \tag{4.9}$$

$$\dot{x}_4 = -7.03268 + 14.52288x_4 - 53.09608x_4^2 + (104.5752\cos(0.08727 - x_3)$$
$$+ 7.84314\sin(0.08727 - x_3))x_4 - 5.22876Q_1 + \left[26.1438x_4\right.$$
$$\times \cos(0.08727 + x_1 - x_3) + 1.96079x_4\sin(0.08727 + x_1 - x_3)\right]u$$
$$- 26.21518x_4^2u^2 \tag{4.10}$$

Here, we choose the load voltage as the system output

$$y = x_4 \tag{4.11}$$

4.1.2 Controller Design

To achieve the main goal − voltage regulation, in the following, we will employ Variable Structure Control (VSC) technique to design controller. As recalled in Chapter 2, it is known that the VSC design procedure consists of two main steps. The first step is to choose a sliding surface, which is a function of system state and desired trajectory. The second step is to design a proper controller to guarantee the state reaching the sliding surface in a finite time and sliding toward the desired trajectory.

The power system has the form

$$\dot{x}_4 = f(x) + g_1(x)u + g_2(x)u^2 \tag{4.12}$$

$$y = x_4 \tag{4.13}$$

Suppose $x_{4d}(t)$ is the desired trajectory. Define the error

$$e(t) = x_4(t) - x_{4d}(t) \tag{4.14}$$

For the VSC design first step, we choose the sliding surface to be $s(t) = 0$ with

$$s(t) = e(t) = 0 \tag{4.15}$$

Clearly, if the system state keeps staying on the sliding surface then the tracking performance can be achieved. That is, $e(t) \to 0 \equiv x_4(t) \to x_{4d}(t)$ as $t \to \infty$.

The second step of VSC design is to design a control law in the form of

$$u = u^{eq} + u^{re} \tag{4.16}$$

To achieve the tracking performance, where u^{re} plays the role of making the error state reach the sliding surface in a finite time and u^{eq} keeps the sliding surface an invariant set and directs the error state to the origin.

As mention in Chapter 2, the condition of forcing system state staying on sliding surface can be written as

$$\dot{s}(t) = 0 \tag{4.17}$$

By solving the above equation formally for the control input, we can obtain the equivalent control, u^{eq} that would maintain $\dot{s} = 0$. Consider the system (4.12), the equivalent control can be chosen as

$$u^{eq} = h(x) \tag{4.18}$$

which $h(x)$ would satisfy

$$\dot{s}(t) = \dot{x}_4 - \dot{x}_{4d}$$
$$= f(x) + g_1(x)h(x) + g_2(x)h(x)^2 - \dot{x}_{4d}$$
$$= 0 \tag{4.19}$$

For voltage regulation, x_{4d} is constant, then $\dot{x}_{4d} = 0$.

From (4.12) ~ (4.17), we can obtain

$$\dot{s}(t) = \dot{x}_4$$

$$= f(x) + g_1(x)(u^{eq} + u^{re}) + g_2(x)(u^{eq} + u^{re})^2$$

$$= f(x) + g_1(x)u^{eq} + g_2(x)(u^{eq})^2 + g_1(x)u^{re} + 2g_2(x)u^{eq}u^{re} + g_2(x)(u^{re})^2$$

$$= [g_1(x) + 2g_2(x)h(x)]u^{re} + g_2(u^{re})^2 \tag{4.20}$$

From (4.18), we have

$$s(t)\dot{s}(t) = s(t) \cdot [(g_1(x) + 2g_2(x)h(x))u^{re} + g_2(u^{re})^2] \tag{4.21}$$

In order to satisfy the sliding condition, we impose the following assumption:

Assumption 1 : During the control period, $g_1(x) + 2g_2(x)h(x) \neq 0$.

From assumption 1, we select

$$u^{re} = \frac{-\eta}{g_1(x) + 2g_2(x)h(x)} sgn(s) \tag{4.22}$$

where $sgn(\cdot)$ is the sign function, and η is a positive number.

It is note that the discontinuity of sign function will cause chattering in the close-loop system. In practice, the sign function $sgn(s)$ is often replace by the saturation function $sat(s)$ where

$$sat(x) = x, \qquad \text{if } |x| \leq 1$$

$$sat(x) = sgn(x), \quad \text{if } |x| \geq 1 \tag{4.23}$$

In order to verify that the control law can satisfy the sliding condition (2.24). We will discuss following possible cases :

A. for $g_2(x) < 0$

(1) $s > 0$, we have

$$s\dot{s} = -\eta|s| + s \cdot g_2(x)(u^{re})^2$$

$$< -\eta|s|, \quad \text{for any given } \eta$$

(2) $s < 0$, we have

$$s\dot{s} = -\eta|s| + s \cdot g_2(x)(u^{re})^2$$

$$= -\eta|s| + \frac{s \cdot g_2(x)}{(g_1(x)+2g_2(x)h(x))^2} \cdot \eta^2$$

To guarantee the sliding condition, we impose the next assumption :

Assumption 2 : $\dfrac{g_2(x)}{(g_1(x)+2g_2(x)h(x))^2}$ is bounded

Then we have,

$$s\dot{s} = -\eta|s| + \frac{s \cdot g_2(x)}{(g_1(x)+2g_2(x)h(x))^2} \cdot \eta^2$$

$$< -k\eta|s|, \quad 0 < k < 1$$

$$\Rightarrow \eta < \frac{(k-1)\cdot(g_1(x)+2g_2(x)h(x))^2}{g_2(x)}$$

B. for $g_2(x) > 0$

(1) $s > 0$

$$s\dot{s} = -\eta|s| + \frac{s \cdot g_2(x)}{(g_1(x)+2g_2(x)h(x))^2} \cdot \eta^2$$

from assumption 2, we have $\quad s\dot{s} < -k\eta|s|, \quad 0 < k < 1$

for $\eta < \dfrac{(1-k)\cdot(g_1(x)+2g_2(x)h(x))^2}{g_2(x)}$

(2) $s < 0$, we have

$$s\dot{s} = -\eta|s| + s \cdot g_2(x)(u^{re})^2$$

$$< -\eta|s|, \quad \text{for any given } \eta$$

So, we know that selecting suitable η, the close-loop system will satisfy sliding condition, that is, the system state will reach the selected sliding surface in a finite time.

4.1.3 Simulation Results

To demonstrate the effect of our designing VSC controller, in this section we use the software "Matlab" as the computational tool to study numerical simulation of the electric power system for voltage regulation.

We consider the power system model (4.7)-(4.11) in the Section 4.1.1. We use the tap changer ratio as the control input signal for the electric power system. The desired voltage level $x_{4d} = 1$. We select sliding surface is $s(t) = x_4(t) - 1$.

By solving $\dot{s}(t) = 0$,

$$\dot{s}(t) = \dot{x}_4 = f(x) + g_1(x)u + g_2(x)u^2 = 0$$

where

$$f(x) = -7.03268 + 14.52288x_4 - 53.09608x_4^2 + (104.5752\cos(0.08727 - x_3)$$

$$+ 7.84314\sin(0.08727 - x_3))x_4 - 5.22876Q_1 - 7.03268$$

$$g_1(x) = 26.1438x_4\cos(0.08727 + x_1 - x_3) + 1.96079x_4\sin(0.08727 + x_1 - x_3)$$

$$g_2(x) = -26.21518x_4^2$$

We can obtain $u = \dfrac{-g_1(x) \pm \sqrt{g_1(x)^2 - 4g_2(x)f(x)}}{2g_2(x)}$, where $u = \dfrac{1}{n}$. n is the tap changer ratio. In practice, the tap changer ratio is positive. Hence, we choose the

equivalent control law, $u^{eq} = \dfrac{-g_1(x) - \sqrt{g_1(x)^2 - 4g_2(x)f(x)}}{2g_2(x)}$ $\qquad$ (4.24)

In this case, $g_2(x) < 0$, and we select

$$u^{re} = \frac{-\eta}{g_1(x) + 2g_2(x)u^{eq}}$$ (4.25)

Hence, the designing control law is

$$u = u^{eq} + u^{re}$$ (4.26)

In this simulation, we select $\eta = 0.1$. Simulation results are given in Figures 4.2-4.5. Figures 4.2 shows the simulation results for the initial state is $x_0 = [0, 0, 0, 1.1]$, and the load reactive power demand Q_1 is constant at 11.2. It is observed that for the initial error is positive (i.e. $s > 0$), it will achieve our desired voltage level by tuning the tap changer ratio. In Figures 4.3, we choose $x_0 = [0.2, 0.2, 0.04, 0.98]$ and assume Q_1 is the same at 11.2. It is clear that for the error is negative, it is also satisfied our main goal - voltage regulation. The same results can also be found in Figure 4.4 and Figure 4.5, while with existence of load variation.

In many practical control problems, the controlled systems may have parameter uncertainty or unknown variation. In our thesis, for the power system, we do not know the load variation of the system actually. With the presence of uncertainty or unknown variation in parameters, the initially controller design may not be able to achieve our desired performance. As in Figure 4.6, in (4.22)~(4.26), we hypothesize the load reactive power demand Q_1 is 11 to our initially controller design. Actually, the load reactive power demand Q_1 is varied with $Q_1 = 11 + 0.1 \sin(3t)$. We can find in Figure 4.6(c), the voltage regulation may not achieve. In worse case, the parameter uncertainty may cause instability. In Figure 4.7(a), we can find that the actual load reactive power demand Q_1 is varied with $Q_1 = 11 + \sin(t)$. For estimated $Q_1 = 11$, we obtain the simulation result in Figure 4.7(c) that not only the desired performance - voltage regulation is not able to achieve but also cause

voltage collapse. So, it is important to reduce the effect of the parameter uncertainty in a system. One way to reduce it is to use parameter estimation. A more detailed discussion of the parameter estimator design is provided in Section 4.2.
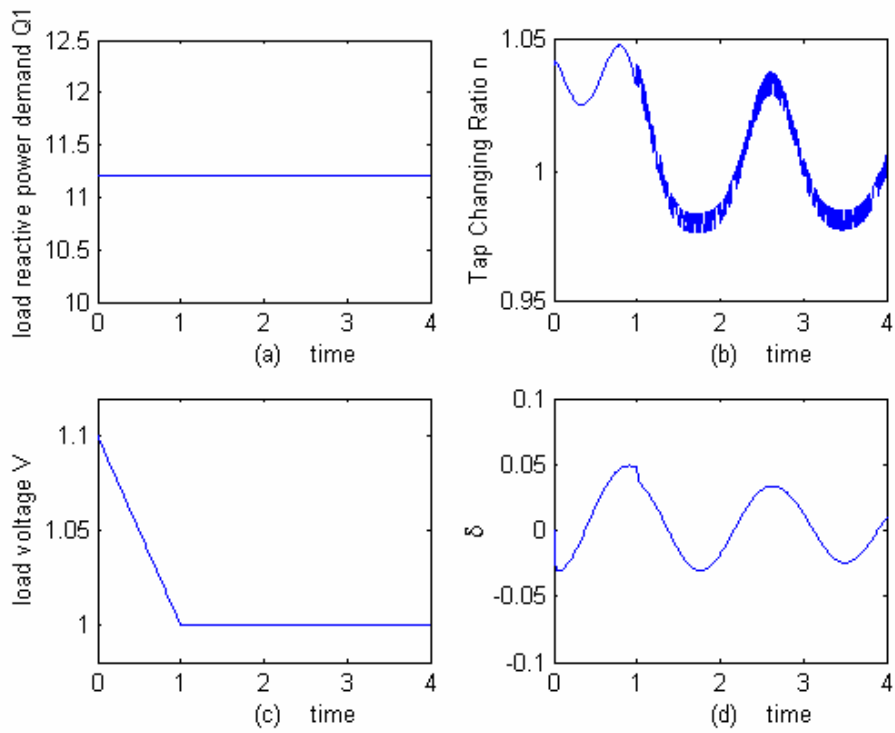
Figures 4.2: $Q_1 = 11.2, x_0 = [0, 0, 0, 1.1]$
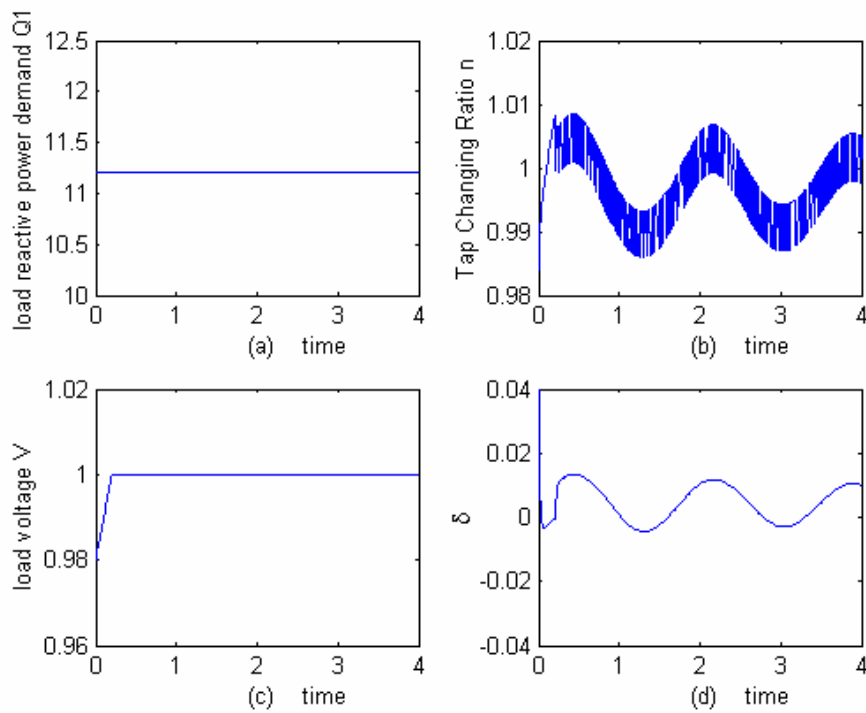
Figures 4.3: $Q_1 = 11.2, x_0 = [0.2, 0.2, 0.04, 0.98]$
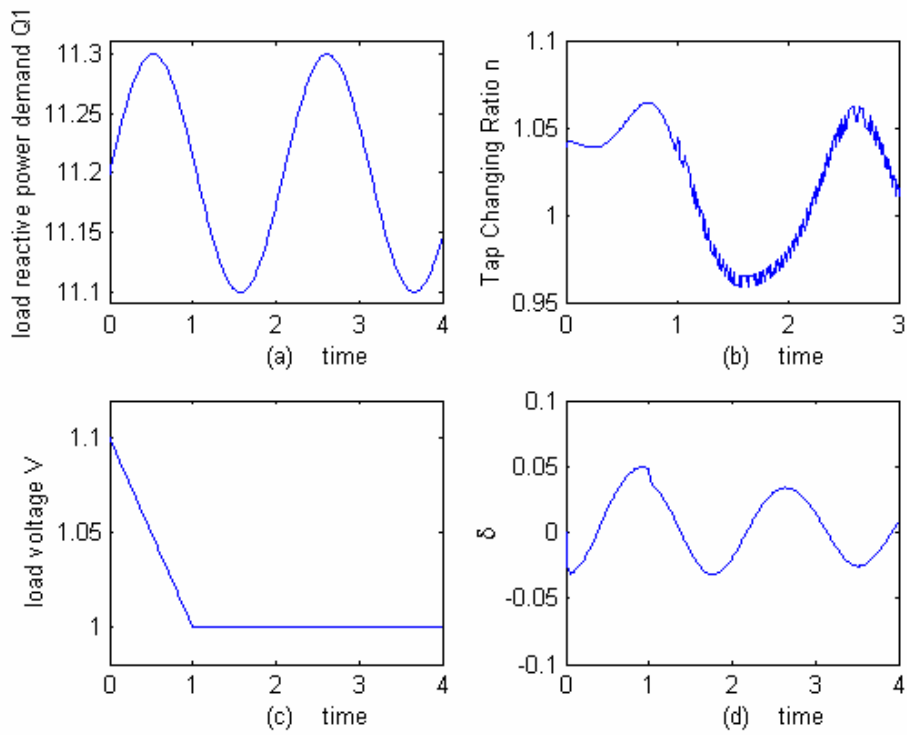
Figure 4.4: $Q_1 = 11.2 + 0.1\sin(3t), x_0 = [0, 0, 0, 1.1]$

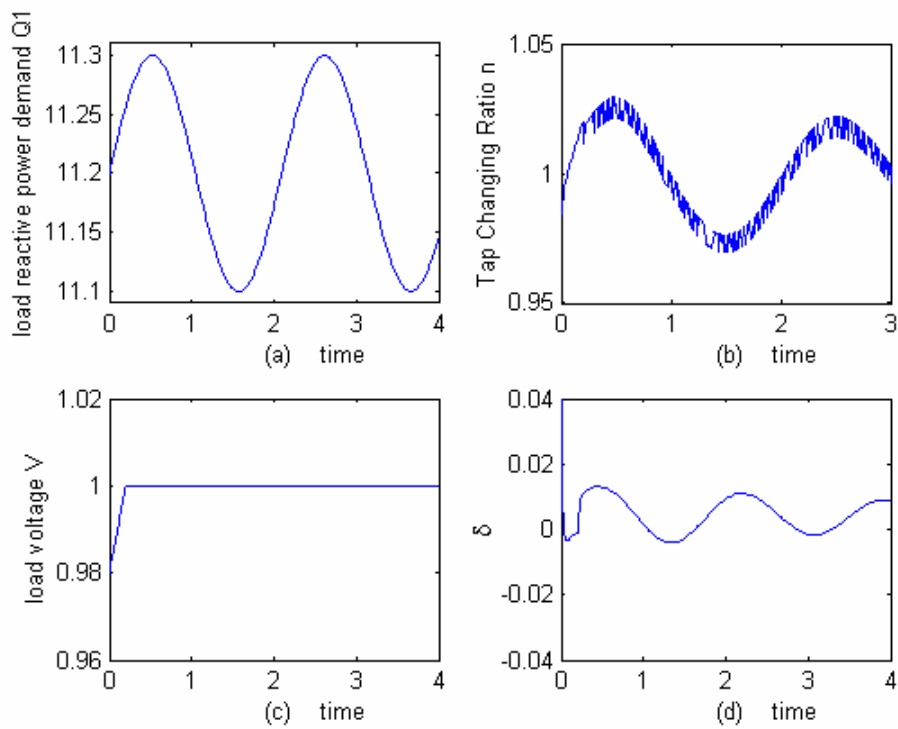
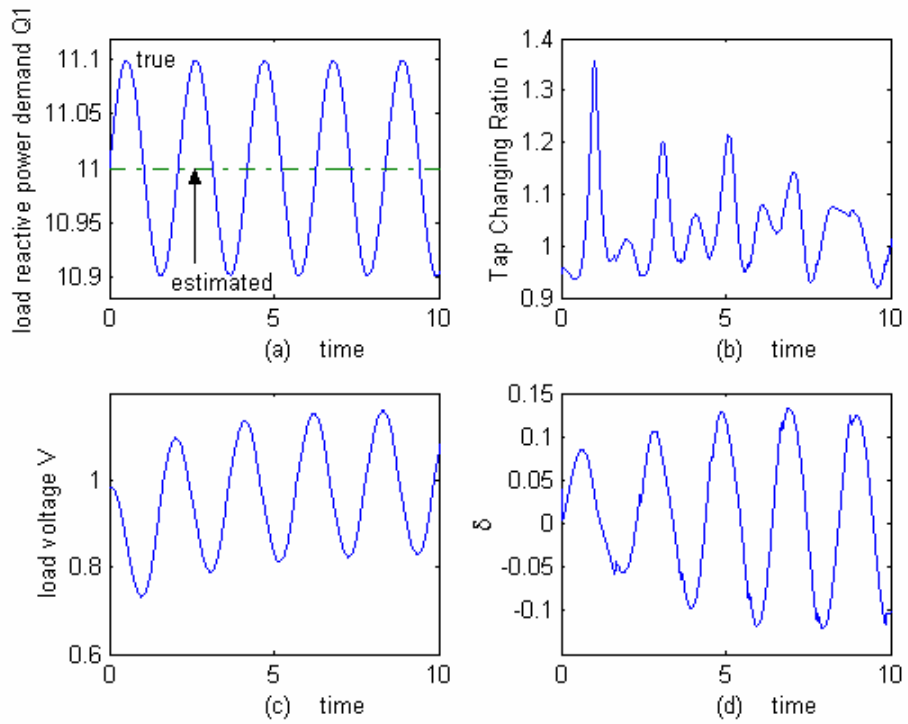Figure 4.5: $Q_1 = 11.2 + 0.1\sin(3t), x_0 = [0.2, 0.2, 0.04, 0.98]$

Figure 4.6 Regulating Performance with Unknown Q_1
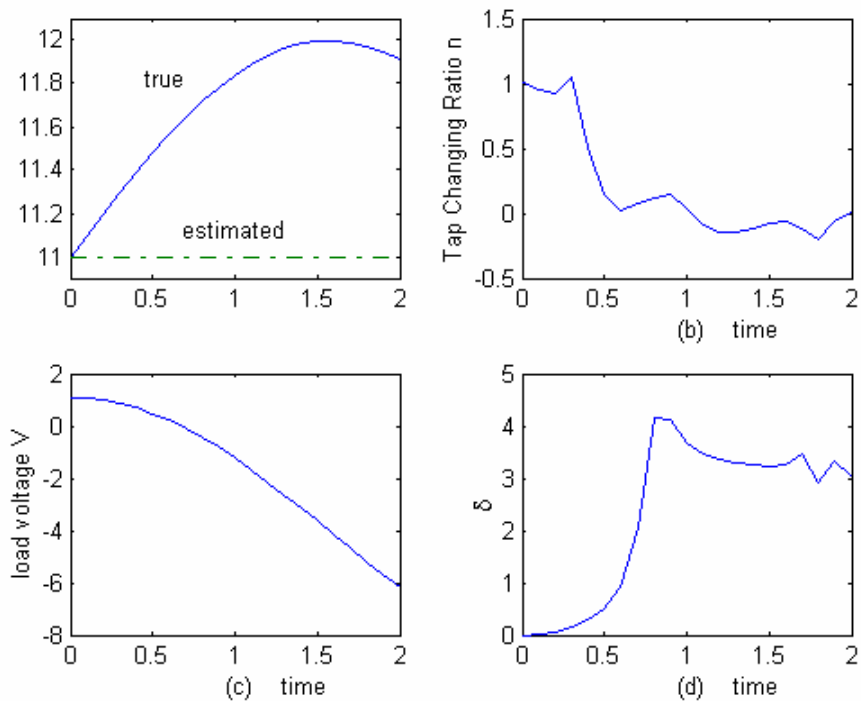
$$x_0 = [0.2, 0.2, 0.04, 0.98]$$

Figure 4.7 Regulating Performance with Unknown Q_1

$$x_0 = [0.2, 0.2, 0.04, 0.98]$$

4.2   Parameter Estimator Design

In practical power system, the system dynamics may have well known dynamics at the beginning, but will experience unpredictable load variation as the control operation goes on. In this section, we will propose two types of load estimator. One is based on gradient method, the other is based on observer approach.

4.2.1   The Gradient Method [25]

4.2.1.1   Linear Parametrization Model

The essence of parameter estimation is to extract parameter information from available data concerning the system. Therefore, we need an estimation model to relate the available data to the unknown parameters, similarly to the familiar experimental data fitting scenario, where we need to hypothesize the form of a curve before finding specific coefficients describing it, based on the data. This estimation model may or may not be the same as the model used for the control purpose. A quite general model for parameter estimation applications is in the linear parametrization from

$$y(t) = W(t)a \tag{4.27}$$

where the n-dimensional vector y contains the "outputs" of the system, the m-dimensional vector a contains unknown parameters to be estimated, and the $n \times m$ matrix $W(t)$ is a signal matrix. Note that both y and W are required to be known form the measurements of the system signals, and thus the only unknown quantities in (4.27) are the parameters in a. This means that (4.27) is simply a linear equation in terms of the unknown a. For every time instant t, there is such an equation. So if we are given the continuous measurements of $y(t)$ and $W(t)$ throughout a time interval, we have an infinite number of equations in the form of

(4.27). If we are given the values of $y(t)$ and $W(t)$ at k sampling instants, we have k sets of such equations instead. The objective of parameter estimation is to simply solve these redundant equations for the m unknown parameters. Clearly, in order to be able to estimate m parameters, we need at least a total of m equations.

4.2.1.2 Predication-Error-Based Estimation Methods

Assume that the parameter vector in (4.27) is unknown, and is estimated to be $\hat{a}(t)$ at time t. One can predict the value of the output $y(t)$ based on the parameter estimate and the model (4.27).

$$\hat{y}(t) = W(t)\hat{a}(t) \tag{4.28}$$

where $\hat{y}$ is called the predicted output at time t. The difference between the predicted output and the measured output y is called the prediction error, denoted by e_1.

$$e_1(t) = \hat{y}(t) - y(t) \tag{4.29}$$

The on-line estimation methods we discuss in this section are based on this error, i.e., the parameter estimation law is driven by e_1. The resulting estimators belong to the so-called prediction-error based estimators, a major class of on-line parameter estimators. The predication error is related to the parameter estimation error, as can be seen from :

$$e_1 = W\hat{a} - Wa = W\tilde{a} \tag{4.30}$$

where $\tilde{a} = \hat{a} - a$ is the parameter estimation error.

The prediction-error based estimations include following methods :

- · Gradient estimation
- · Standard least-squares estimation
- · Least-squares with exponential forgetting
- · A particular method of variable exponential forgetting

In order to simplify the calculation and make the parameters be estimated fast, we adopt gradient estimation as load estimator for the power system in our thesis. In the following section, we take brief introduction to the gradient estimation.

4.2.1.3 The Gradient Estimator

The basic idea in gradient estimation is that the parameters should be updated so that the prediction error is reduced. This idea is implemented by updating the parameters in the converse direction of the gradient of the squared prediction error with respect to the parameters.

$$\dot{\hat{a}} = -\frac{1}{2}p_o\frac{\partial[e_1^Te_1]}{\partial\hat{a}} \tag{4.31}$$

Where p_o is a positive number called the estimator gain. In view of (4.28) and (4.29), this can be written as

$$\dot{\hat{a}} = -p_oW^Te_1 \tag{4.32}$$

To see the properties of this estimator, we use (4.32) and (4.30) to obtain

$$\dot{\hat{a}} = -p_oW^TW\tilde{a} \tag{4.33}$$

Using the Lyapunov function candidate

$$V = \tilde{a}^T\tilde{a} \tag{4.34}$$

its derivative is easily found to be

$$\dot{V} = -2p_o\tilde{a}^TW^TW\tilde{a} \leqslant 0$$

This implies that the gradient estimator is always stable. By noting that V is actually the squared parameter error, we see that the magnitude of the parameter error is always decreasing. However, the convergence of the estimated parameters to the true parameters depends on the excitation of the signals.

It is noted that in the convergence analysis of gradient estimator, we only consider that the true parameters are constant.

4.2.1.4 Application To Power Systems

Let us consider our power system dynamics (4.7)~(4.11)

$$\dot{y} = \dot{x}_4$$
$$= F(x, u) - 5.22876Q_1 \tag{4.35}$$

where

$$F(x, u) = -7.03268 + 14.52288x_4 - 53.09608x_4^2$$

$$+ (104.5752\cos(0.08727 - x_3) + 7.84314\sin(0.08727 - x_3))x_4$$

$$+ \big[26.1438x_4\cos(0.08727 + x_1 - x_3)$$

$$+ 1.96079x_4\sin(0.08727 + x_1 - x_3)\big]u$$

$$- 26.21518x_4^2u^2$$

Assume that Q_1 in the model is unknown. The above model cannot be directly used for estimation, because the derivative of y appears in the above equation. To eliminate $\dot{y}$ in the above equation, let us take Laplace transform of both sides

$$SY - y(0) = L\{F(x, u)\} - 5.22876L\{Q_1\} \tag{4.36}$$

Rearranging (4.36)

$$(S + \lambda_f)Y - \lambda_f Y - y(0) = L\{F(x, u)\} - 5.22876L\{Q_1\}$$

where S is the Laplace operator and λ_f is a positive constant

$$\Rightarrow \qquad Y = \frac{1}{S+\lambda_f}[L\{F(x, u)\} + \lambda_f Y + y(0) - 5.22876L\{Q_1\}]$$

$$\Rightarrow \qquad y(t) = \frac{1}{S+\lambda_f}\big[F(x, u) + \lambda_f y + y(0) - 5.22876\big]\begin{bmatrix} 1 \\ Q_1 \end{bmatrix} \tag{4.37}$$

This leads (4.37) to the form of linear parametrization form of (4.27) with

$$W(t) = \frac{1}{S+\lambda_f}\big[F(x, u) + \lambda y + y(0) - 5.22876\big]$$

$$a(t) = \begin{bmatrix} 1 \\ Q_1 \end{bmatrix}$$

In the following, we use gradient estimator to estimate the load variation in the power system with output being described by (4.35). As shown in Figure 4.8. The true load reactive power demand is assumed to be $Q_1 = 11$. We let $p_o = 10$ and $\lambda_f = 10$ and the initial condition is $x_0 = [0, 0, 0, 1.1]$. It is clear that the parameter error will converge to zero for a finite time. It is noted that the choices of estimation gain p_o, initial state x_0, and the λ_f of filter have a fundamental influence on the convergence behavior of the estimator. Generally speaking, increasing p_o and λ_f leads to faster parameter convergence, especially for increasing λ_f as shown in Figure 4.9. In the next, we consider the parameter Q_1 is slowly time-varying, with $Q_1 = 11 + 0.1\sin(0.5t)$ and p_o, λ_f, x_0, we take the same as in Figure 4.8. It is seen in Figure 4.10 that the gradient method may work well in the presence of parameter variation. However, if the true parameters vary fast, it is hard for gradient estimator to estimate accurately. It can be seen in Figure 4.11 with fast time-varying Q_1 for $Q_1 = 11 + 0.1\sin(5t)$. Obviously, the estimate is poor.

Figure 4.8: Estimation for constant load $Q_1 \equiv 11$ by Gradient method

with $\lambda_f = 10$ and $p_o = 10$

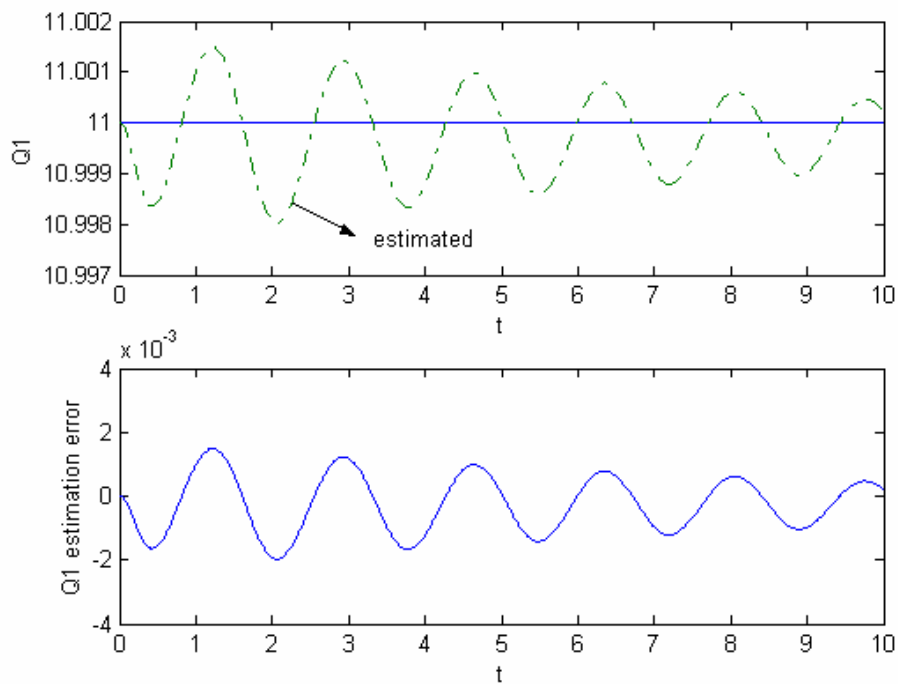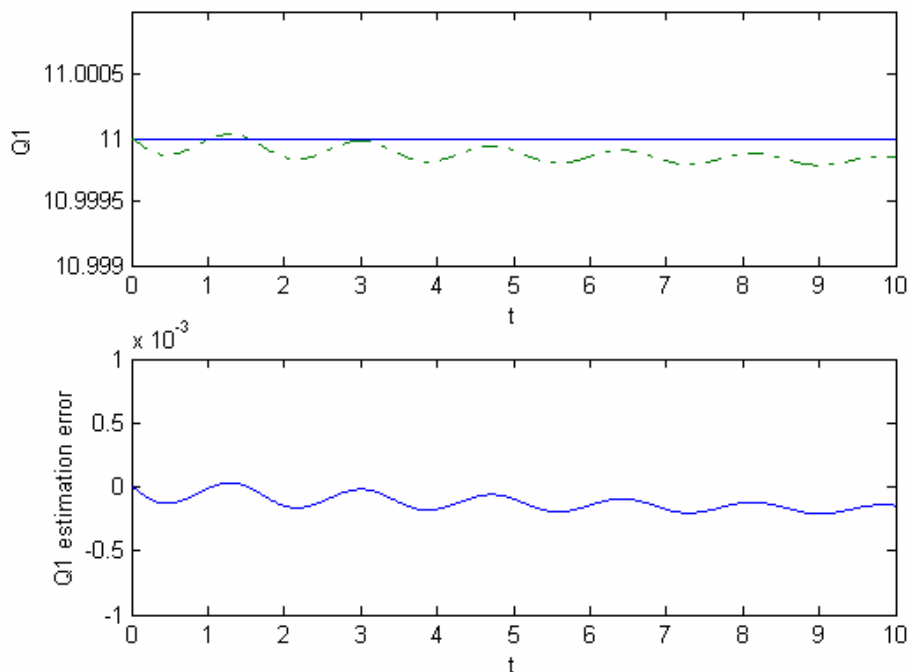
Figure: 4.9: Estimation for constant load $Q_1 \equiv 11$ by Gradient method
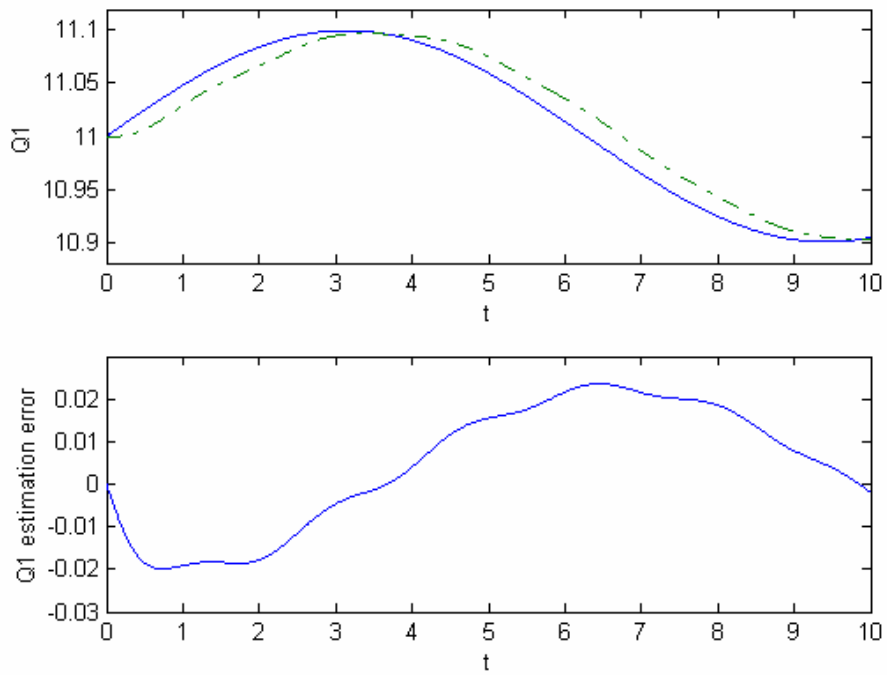
with $\lambda_f = 50$ and $p_o = 10$

Figure 4.10: Estimation for slow time-varying load $Q_1 \equiv 11 + 0.1\sin(0.5t)$
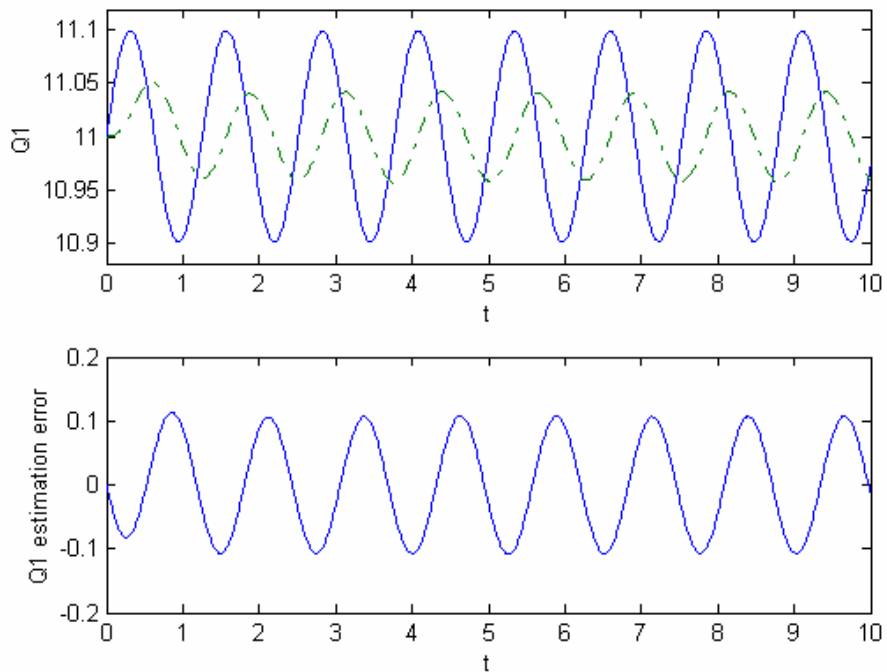
by Gradient method with $\lambda_f = 10$ and $p_o = 10$

Figure 4.11: Estimation for fast time-varying load $Q_1 \equiv 11 + 0.1\sin(5t)$

by Gradient method with $\lambda_f = 10$ and $p_o = 10$

4.2.2 An Observer Approach

The main goal of this section is to design a parameter observer that can real-time estimate the variation of the system parameter.

4.2.2.1 The Transformation of Decoupled Form

From the power system dynamics (4.1)~(4.6), the power system dynamics has four states $x = (\delta_m \;\; \omega \;\; \delta \;\; V)^T$, and one control $u = \frac{1}{n}$. We assume that all the states are measurable and P_1, Q_1 are system's unknown parameters. Then, the power system dynamics has the following form :

$$\dot{x} = f(x, u) + g(x)a \tag{4.38}$$

where $a = \begin{pmatrix} Q_1 \\ P_1 \end{pmatrix}$ and $g(x) = \begin{pmatrix} 0 & 0 \\ 0 & 0 \\ g_{11} & g_{12} \\ g_{21} & g_{22} \end{pmatrix}$

It is clear from (4.38) that the unknown parameters only appear in the state equations of $\dot{x}_3$, $\dot{x}_4$ and $g(x)$ has rank 2. In order to obtain our desired decouple form, we make the following state transformation.

$$z = \bar{M}x \tag{4.39}$$

with

$$\bar{M} = \begin{pmatrix} I_{2\times2} & 0 \\ 0 & M_{2\times2} \end{pmatrix} \tag{4.40}$$

$$M_{2\times2} = \begin{pmatrix} g_{11} & g_{12} \\ g_{21} & g_{22} \end{pmatrix}^{-1} \tag{4.41}$$

The state equations in new state variables are described as below

$$\dot{z} = \bar{M}\dot{x} = \bar{M}f(x, u) + \bar{M}g(x)a$$
$$= \bar{M}f(\bar{M}^{-1}z, u) + \bar{M}g(x)a$$
$$= f_{new}(z, u) + \bar{M}g(x)a \tag{4.42}$$

where $f_{new}(z, u)$ and $\bar{M}g(x)$ are given by

$$f_{new}(z, u) = \begin{pmatrix} f_{1\ new}(z, u) \\ f_{2\ new}(z, u) \\ f_{3\ new}(z, u) \\ f_{4\ new}(z, u) \end{pmatrix} \qquad (4.43)$$

and $\bar{M}g(x) = \begin{pmatrix} 0 & 0 \\ 0 & 0 \\ 1 & 0 \\ 0 & 1 \end{pmatrix}$ \qquad (4.44)

Under these settings, we have new state equations

$$\dot{z}_1 = f_{1\ new}(z, u)$$

$$\dot{z}_2 = f_{2\ new}(z, u)$$

$$\dot{z}_3 = f_{3\ new}(z, u) + Q_1$$

$$\dot{z}_4 = f_{4\ new}(z, u) + P_1 \qquad (4.45)$$

Clearly, Q_1 only appear in the state equation of $\dot{z}_3$, similarly P_1 only appear in the state equation of $\dot{z}_4$. It makes it easy for us that to design parameter observer. The details are discussed in the next section.

4.2.2.2 Observer Design for Constant Parameters

With the aid of transformed system (4.45), we will design a parameter observer that can real-time estimate the variation of the system parameter. At first, we assume that the true parameters are constant to design the observer in this section. However, the true parameters may be time varying. We will discuss the observer for time-varying parameters in the next section.

For the true parameters are constant, we design the observer and error signal as follows :

$$\dot{\xi}_1 = f_{3\ new}(z, u) + Q_{1n} + k_1(z_3 - \xi_1)$$

$$\dot{\xi}_2 = f_{4\ new}(z, u) + P_{1n} + k_2(z_4 - \xi_2) \tag{4.46}$$

$$e_1 = z_3 - \xi_1$$

$$e_2 = z_4 - \xi_2 \tag{4.47}$$

Here, $k_i > 0$ for $i = 1, 2$. Q_{1n} and P_{1n} are considered as the constant nominal values of Q_1 and P_1. The difference between the nominal and actual parameter values is called the parameter estimated error, denoted by

$$m_1 = Q_1 - \hat{Q}_1 \tag{4.48}$$

$$m_2 = P_1 - \hat{P}_1 \tag{4.49}$$

We design the estimated parameter as follow:

$$\hat{Q}_1 = k_1 e_1 + Q_{1n} \tag{4.50}$$

$$\hat{P}_1 = k_2 e_2 + P_{1n} \tag{4.51}$$

Under this design, we will obtain the unknown parameters by the way of to observe the value of error signal. The details are given as follows :

From (4.46)、(4.47)、(4.48), we can obtain

$$e_1 = z_3 - \xi_1$$

$$\Rightarrow \dot{e}_1 = \dot{z}_3 - \dot{\xi}_1$$

$$= f_{3\ new}(z, u) + Q_1 - (f_{3\ new}(z, u) + Q_{1n} + k_1(z_3 - \xi_1))$$

$$\Rightarrow \dot{e}_1 = -k_1 e_1 + (Q_1 - Q_{1n}) \tag{4.52}$$

Since k_1 is assumed to be a positive constant, and m_1 is constant for Q_1 is constant. Thus, e_1 will approach $\frac{Q_1 - Q_{1n}}{k_1}$ after a short time transient.

$$e_1 \simeq \frac{Q_1 - Q_{1n}}{k_1}$$

Then,

$$Q_1 \simeq k_1 e_1 + Q_{1n} \tag{4.53}$$

Obviously, $\hat{Q}_1$ will approach Q_1 after a short time transient. Thus the actual parameter value can be obtained by (4.50). The other case can be similarly derived.

For $e_2 = z_4 - \xi_2$

$$\Rightarrow \quad \dot{e}_2 = \dot{z}_4 - \dot{\xi}_2$$

$$= f_{4\ new}(z, u) + P_1 - (f_{4\ new}(z, u) + P_{1n} + k_2(z_4 - \xi_2))$$

$$\Rightarrow \quad \dot{e}_2 = -k_2 e_2 + (P_1 - P_{1n}) \tag{4.54}$$

After a short time transient, e_2 will approach $\frac{P_1 - P_{1n}}{k_2}$. It follows :

$$e_2 \simeq \frac{P_1 - P_{1n}}{k_2}$$

$$\Rightarrow \quad P_1 \simeq k_2 e_2 + P_{1n}$$

$$= \hat{P}_1 \tag{4.55}$$

It is noted that in order to have good estimation performance, the initial parameter estimates should be chosen to be as accurate as possible. Furthermore, if the true parameters vary, it is possible for the parameter observer to estimate accurately for k_i large enough. It can be found in the examples in Section 4.2.2.4.

4.2.2.3 Observer Design for Time-Varying Parameters

In this section, we will design a parameter observer to deal with time-varying parameters. It may guarantee to obtain good parameter estimation, even though the true parameters vary fast. The idea is similar to that in Section 4.2.2.2.

With the aid of transformed system (4.45), we design the observer and error signal as follows :

$$\dot{\xi}_1 = f_3{}_{new}(z, u) + \hat{Q}_1 + k_1(z_3 - \xi_1)$$

$$\dot{\xi}_2 = f_4{}_{new}(z, u) + \hat{P}_1 + k_2(z_4 - \xi_2) \qquad (4.56)$$

$$e_1 = z_3 - \xi_1$$

$$e_2 = z_4 - \xi_2 \qquad (4.57)$$

Here, $k_i > 0$ for $i = 1, 2$. $\hat{Q}_1$ and $\hat{P}_1$ are estimated values of Q_1 and P_1. The difference between the estimated and actual parameter values is called the parameter estimated error, denoted by

$$m_1 = Q_1 - \hat{Q}_1 \qquad (4.58)$$

$$m_2 = P_1 - \hat{P}_1 \qquad (4.59)$$

and the true parameters $Q_1 \cdot P_1$ can be written as

$$Q_1 = Q_{1n} + \triangle Q \qquad (4.60)$$

$$P_1 = P_{1n} + \triangle P \qquad (4.61)$$

where Q_{1n} and P_{1n} are considered as the constant nominal values of Q_1 and P_1. $\triangle Q$ and $\triangle P$ are the variation of Q_1 and P_1. Assume that the variations of parameters vary at the small region, i.e. $\|\triangle Q\| < \rho$ and $\|\triangle P\| < \rho$.

Then, we design the estimated parameter as follow:

$$\hat{Q}_1 = Q_{1n} - k_1 e_1 + (\rho + \eta) \, sat(\tfrac{e_1}{\phi}) \qquad (4.62)$$

$$\hat{P}_1 = P_{1n} - k_2 e_2 + (\rho + \eta) \, sat(\tfrac{e_2}{\phi}) \qquad (4.63)$$

where, ϕ is the boundary layer of the saturation function.

Under this design, we will obtain the unknown parameters by the way of to observe the value of error signal. The details are given as follows :

First, we select the sliding surface $s = e_1$. From (4.56)、(4.57)、(4.58), we can obtain

$$e_1 = z_3 - \xi_1$$

$$\Rightarrow \ \dot{e}_1 = \dot{z}_3 - \dot{\xi}_1$$

$$= f_{3 \ new}(z, u) + Q_1 - (f_{3 \ new}(z, u) + \hat{Q}_1 + k_1(z_3 - \xi_1))$$

$$\Rightarrow \ \dot{e}_1 = -k_1 e_1 + \left(Q_1 - \hat{Q}_1\right)$$

$$= -k_1 e_1 + \left(Q_{1n} + \triangle Q - \hat{Q}_1\right) \tag{4.64}$$

For $s = e_1$

$$\Rightarrow \ s\dot{s} = e_1^T(-k_1 e_1 + Q_{1n} + \triangle Q - \hat{Q}_1) \tag{4.65}$$

It is known that $\|\triangle Q\| < \rho$. Hence, we design the estimated parameter $\hat{Q}_1$ as follow:

$$\hat{Q}_1 = Q_{1n} - k_1 e_1 + (\rho + \eta) \, sat(\tfrac{e_1}{\phi}) \tag{4.66}$$

From (4.65) and (4.66), we get

$$s\dot{s} = e_1^T \left[\triangle Q - (\rho + \eta) \, sat(\tfrac{e_1}{\phi}) \right] \tag{4.67}$$

$$\Rightarrow \ s\dot{s} \le -\eta \, |s| \tag{4.68}$$

Satisfying (4.58) guarantees that the error signal e_1 will approach to zero in a finite time.

If $e_1 \to 0$ & smooth enough $\left(\dot{e}_1 \to 0\right)$, then from (4.64) we can obtain $\left(Q_1 - \hat{Q}_1\right) \to 0$ in a finite time.

The other case can be similarly derived. Details are omitted.

4.2.2.4 Application to Power Systems

Let us consider our power system dynamics (4.1)~(4.10). In order to make observer designing simpler, we rewrite power system dynamics in the form of (4.38) with the actual system parameters.

$$\begin{pmatrix} \dot{x}_1 \\ \dot{x}_2 \\ \dot{x}_3 \\ \dot{x}_4 \end{pmatrix} = \begin{pmatrix} f_1(x,u) \\ f_2(x,u) \\ f_3(x,u) \\ f_4(x,u) \end{pmatrix} + \begin{pmatrix} 0 & 0 \\ 0 & 0 \\ 33.33333 & 0 \\ -5.22876 & -0.39216 \end{pmatrix} \begin{pmatrix} Q_1 \\ P_1 \end{pmatrix} \qquad (4.69)$$

We select a variable transformed matrix $\bar{M}$

$$\bar{M} = \begin{pmatrix} 1 & 0 & 0 & 0 \\ 0 & 1 & 0 & 0 \\ 0 & 0 & 0.03 & 0 \\ 0 & 0 & -0.4 & -2.55 \end{pmatrix} \qquad (4.70)$$

And we set new state variables $z = \bar{M}x$. After state transformation, we can obtain

the new system equations :

$$\dot{z} = \bar{M}\dot{x}$$

$$= \bar{M}f(x,u) + \bar{M}g(x) \begin{pmatrix} Q_1 \\ P_1 \end{pmatrix} \qquad (4.71)$$

$$\Rightarrow$$

$$\dot{z}_1 = f_1(x,u)$$

$$\dot{z}_2 = f_2(x,u)$$

$$\dot{z}_3 = 0.03 f_3(x,u) + Q_1$$

$$\dot{z}_4 = -0.4 f_3(x,u) - 2.55 f_4(x,u) + P_1 \qquad (4.72)$$

In the practical power system, the variation of reactive power demand is often greater than real power demand. In these simulations, we will show the estimation performance of Q_1. Similarly, P_1 can obtain at same procedures.

In the following simulations, we will discuss the estimation of reactive power demand of PQ-load Q_1 under the situation of $P_1 = 0$ and $u = 1$.

First, we consider the true reactive power demand of load in the uncontrolled

power system is constant, we design parameter observer as follow :

$$\dot{\xi}_1 = 0.03 f_3(x, u) + Q_{1n} + k_1(z_3 - \xi_1) \tag{4.73}$$

The error signals are

$$e_1 = z_3 - \xi_1 \tag{4.74}$$

The estimated parameter is designed as follow:

$$\hat{Q}_1 = Q_{1n} + k_1 e_1 \tag{4.75}$$

As discussion in Section 4.2.2.2, the estimated parameter $\hat{Q}_1$ will approach the true

parameter Q_1 in a short time transient.

Simulations of constant parameter are provided in Figures 4.12 and 4.13. Here, We

consider the true reactive power demand of load in the uncontrolled power system is

$Q_1 = 11$ under the situation of the system initial state $x_0 = [0, 0, 0, 1.1]$. We set

the nominal parameter value of parameter observer, $Q_{1n} = 11$, and select $k_1 = 10$.

The estimation performance is displayed in Figure 4.12. It is seen that the estimated

parameter will approach actual parameter as expected. Figure 4.13 shows the results

when the true reactive power demand of load is $Q_1 = 12$ with initial state being

$x_0 = [0, 0, 0, 1.1]$ and $Q_{1n} = 9 \cdot k_1 = 10$. It is clear that estimated error may

converge to zero.

In addition, in order to have good estimation performance, the nominal parameter

value of the observer should be chosen to be as accurate as possible. The result can

compare the estimated performance in Figure 4.12 with that in Figure 4.13. Accurate

initial parameter estimates may lead to fast parameter convergence.

In the next, let us consider the estimated performance of the prior designing

parameter observer in the presence of parameter variation. First, in the presence of

relative slow load variation in the power system, $Q_1 = 11 + 0.1 \sin(t)$, we select

$Q_{1n} = 11$ and $k_1 = 10$. The estimated and true parameters are shown in Figure 4.14. It is seen that the designing parameter observer works well in the presence of slow parameter variation. Then, let us consider that if the true parameter varies faster, what estimated performance will become? To see this, we let the load variation in the power system varying with relative high frequency, which $Q_1 = 11 + 0.1\sin(10t)$, and selecting $Q_{1n} = 11$ and $k_1 = 10$. The simulation result is shown in Figure 4.15. We can find the gain k_1 is not large enough so that the parameter variation can not be tracked sufficiently accurately. Thus, we choose larger k_1 for $k_1 = 50$ with the same varied frequency in the Figure 4.16. It is seen that the estimation performance will improve by increasing k_1.

Finally, Let us consider the observer designing in the Section 4.2.2.3. Its estimation performance may be better with prior one, especially in the presence of fast parameter variation.

Let us consider the true reactive power demand of load in the uncontrolled power system is vary, we design parameter observer as follow :

$$\dot{\xi}_1 = 0.03f_3(x, u) + \hat{Q}_1 + k_1(z_3 - \xi_1) \tag{4.76}$$

The error signals are

$$e_1 = z_3 - \xi_1 \tag{4.77}$$

With the variation of Q_1, Q_1 can be written as

$$Q_1 = Q_{1n} + \triangle Q \tag{4.78}$$

We design the estimated parameter as follow:

$$\hat{Q}_1 = Q_{1n} - k_1 e_1 + (\rho + \eta)\,sat(\tfrac{e_1}{\phi}) \tag{4.79}$$

Figures 4.17~4.18 show the estimation performance of different time-varying frequency of the load variation. In these simulations, the design parameters are taken

to be $k_1 = 1$, $Q_{1n} = 11$, $\rho = 0.2$, $\eta = 0.01$, $\phi = 0.001$ under the situation of the system initial state $x_0 = [0, 0, 0, 1.1]$. It is clear that it works quite well in the presence of fast parameter variation, even though the parameter vary faster.

Finally, let us consider the situation about a 5% load variation. Figure 4.19 shows the estimation result of a 5% load variation about the operating point. The variation of reactive power demand is shown in Figure 4.19(a). It is seen that the estimated performance is also well.

We have discussed two types of estimators in this section. The gradient estimator has the drawback of slow convergence [25]. If the true load vary fast, it is harder for gradient estimator to estimate accurately. We have developed an observer approach to overcome the problem of convergence speed in Section 4.2. The following simulation will compare the convergence behavior of two estimators in the presence of load variation. We suppose the true load is time-varying, with $Q_1 = 11 + 0.1\sin(5t)$. The initial condition of power system is $x_0 = [0, 0, 0, 1.1]$. And the design parameters are taken to be $p_o = 10$, $\lambda_f = 10$ and $k_1 = 1$, $Q_{1n} = 11$, $\rho = 0.2$, $\eta = 0.01$, $\phi = 0.001$, respectively. Figures 4.20~4.21 show the estimation performances of two methods. Obviously, the observer approach has faster convergence than gradient method.
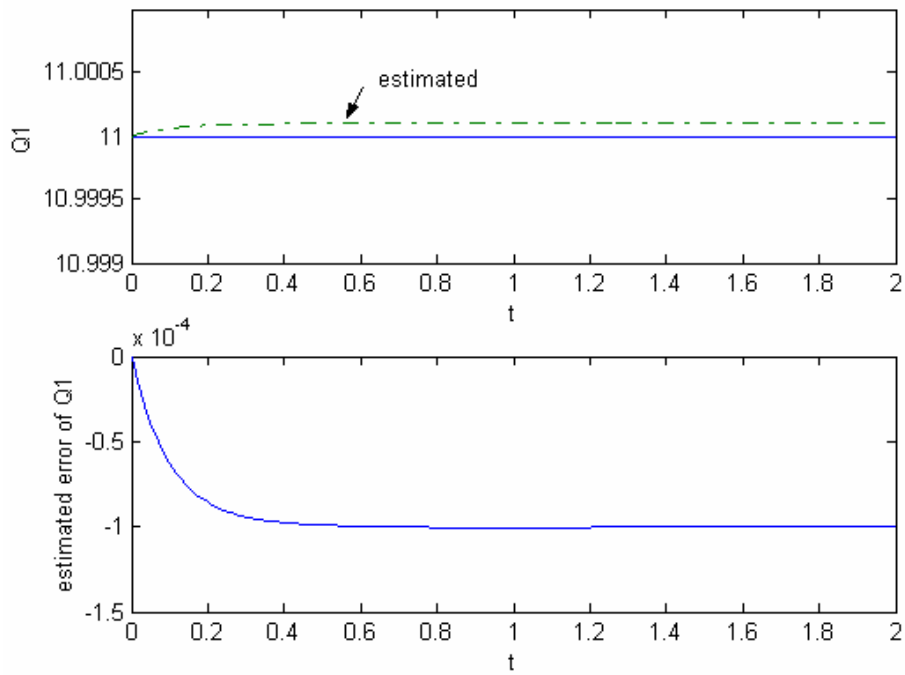
Figure 4.12: Estimation result by observer method for $Q_1 = 11$

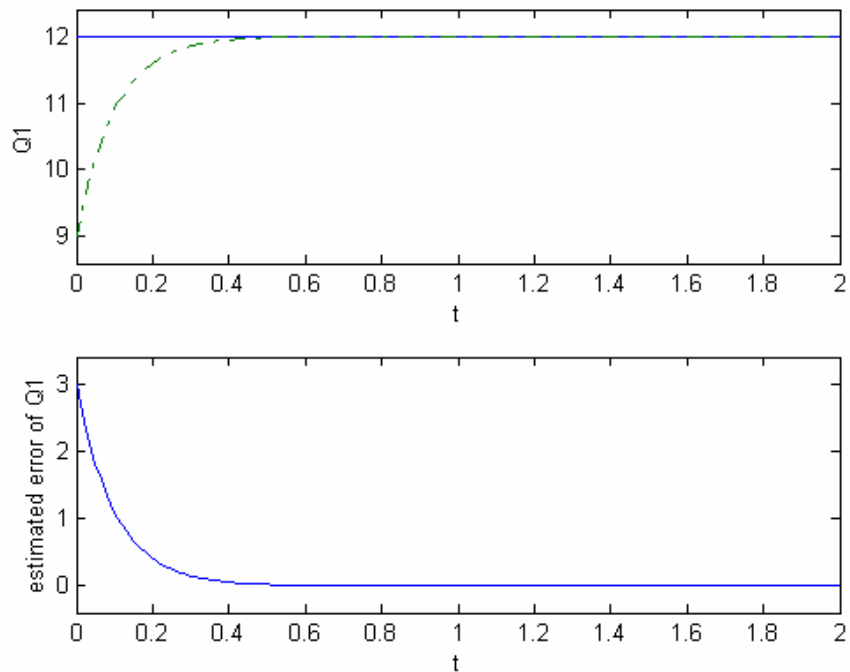and $k_1 = 10, \ Q_{1n} = 11$

Figure 4.13: Estimation result by observer method for $Q_1 = 12$
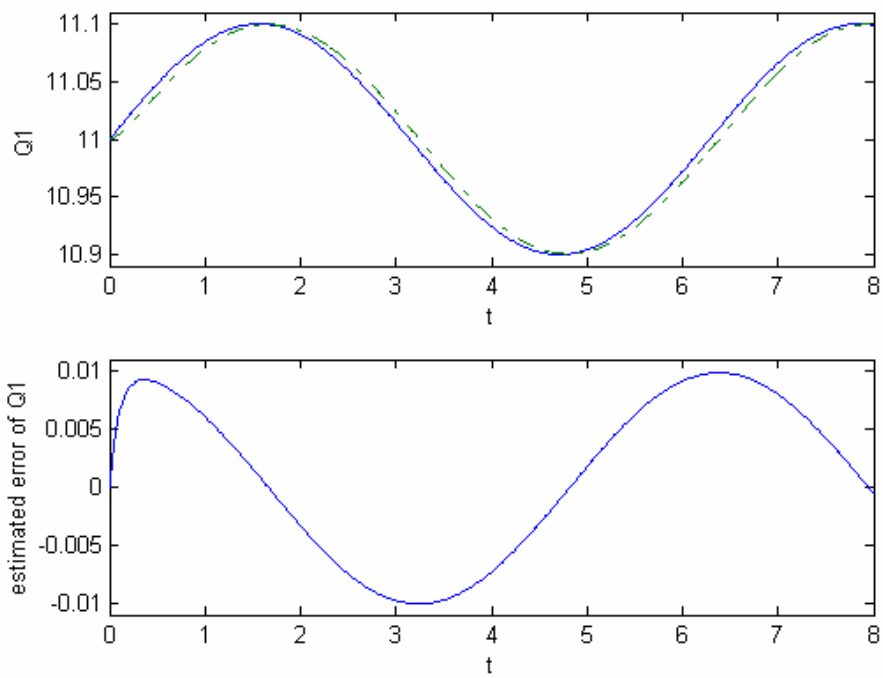
and $k_1 = 10, \ Q_{1n} = 9$

Figure 4.14: Estimation result by observer method for $Q_1 = 11 + 0.1\sin(t)$

and $k_1 = 10$, $Q_{1n} = 11$

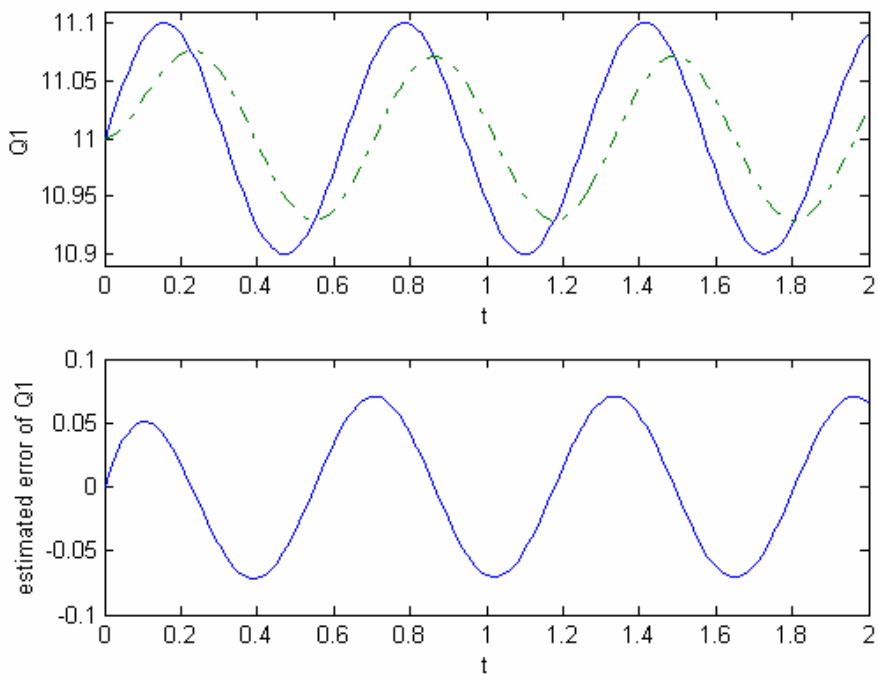
Figure 4.15: Estimation result by observer method for $Q_1 = 11 + 0.1\sin(10t)$
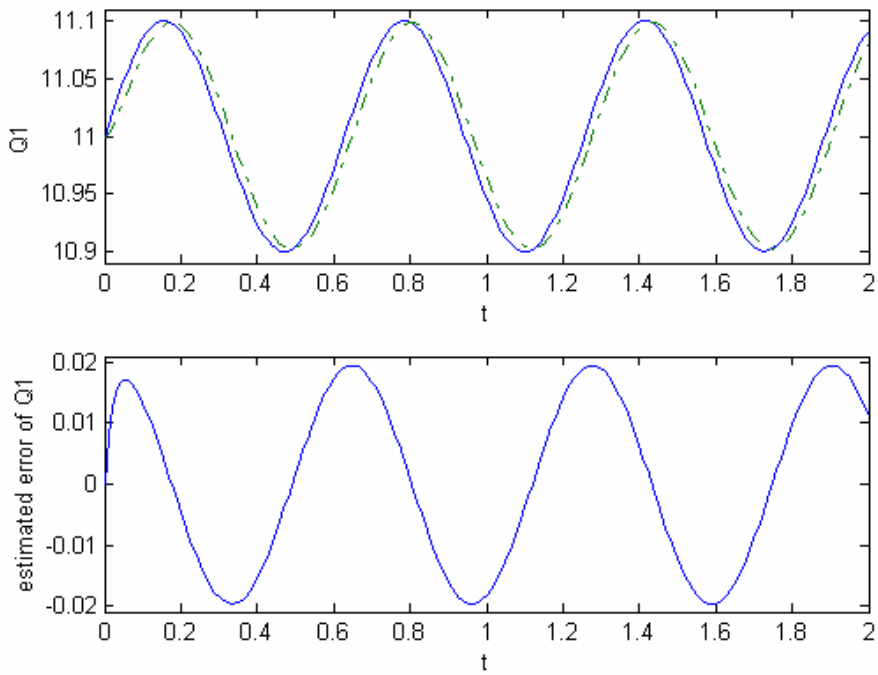
and $k_1 = 10$, $Q_{1n} = 11$

Figure 4.16: Estimation result by observer method for $Q_1 = 11 + 0.1\sin(10t)$
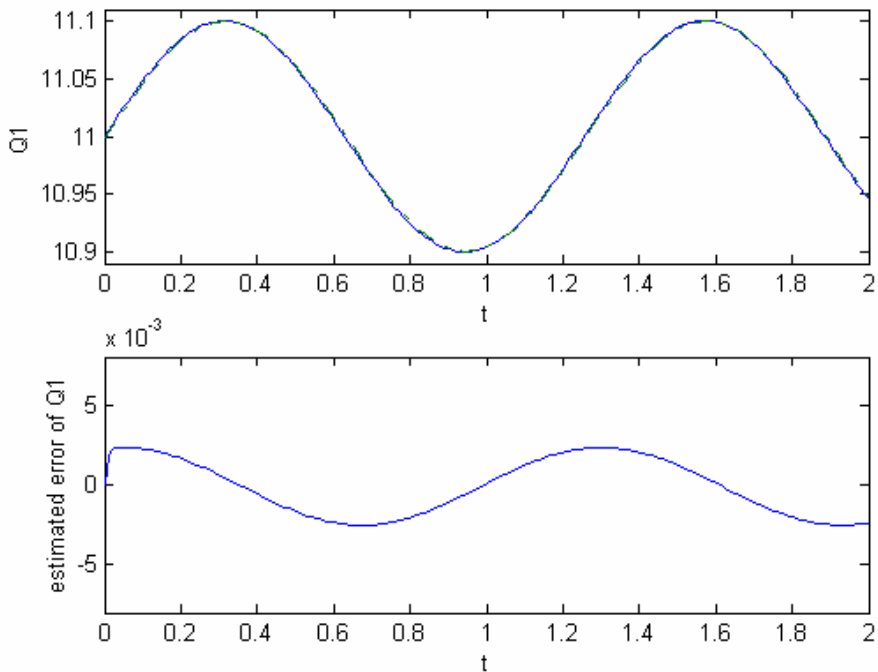
and $k_1 = 50$, $Q_{1n} = 11$

Figure 4.17: Estimation result by observer method for $Q_1 = 11 + 0.1\sin(5t)$

and $k_1 = 1$, $Q_{1n} = 11$, $\rho = 0.2$, $\eta = 0.01$, $\phi = 0.001$

Figure 4.18: Estimation result by observer method for $Q_1 = 11 + 0.1\sin(10t)$

and $k_1 = 1$, $Q_{1n} = 11$, $\rho = 0.2$, $\eta = 0.01$, $\phi = 0.001$

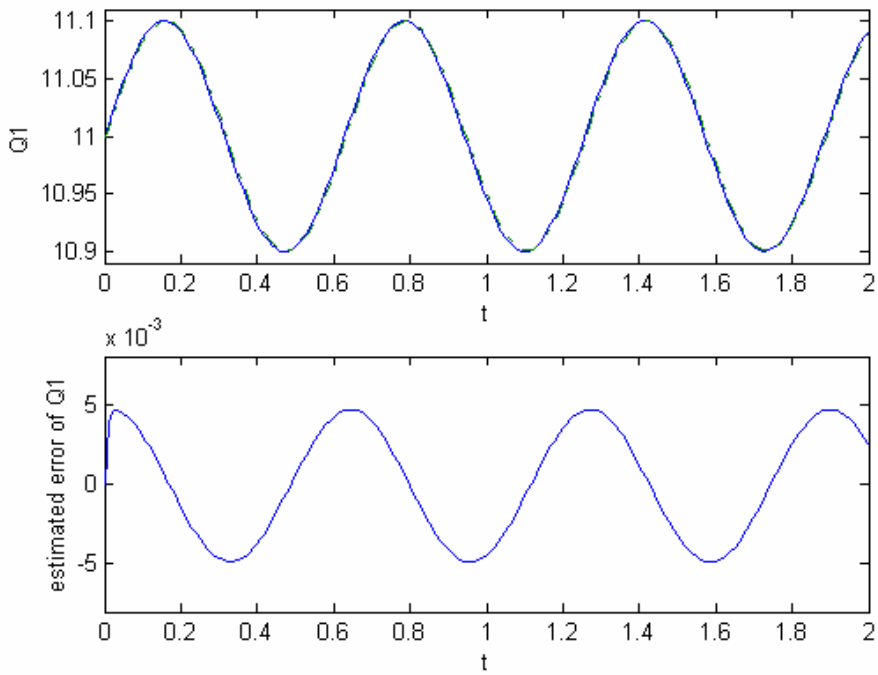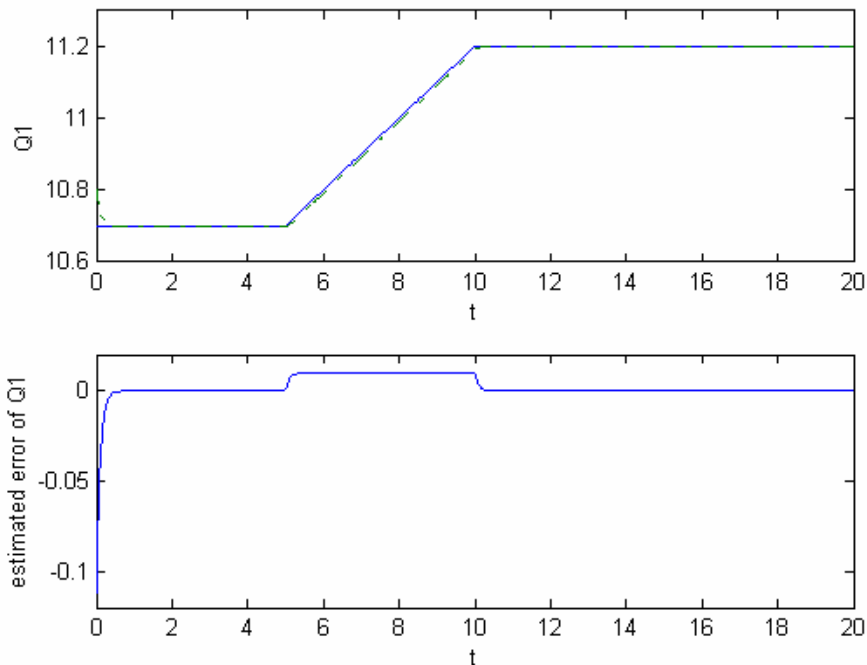Figure 4.19: Estimation result by observer method for 5% variation of Q_1

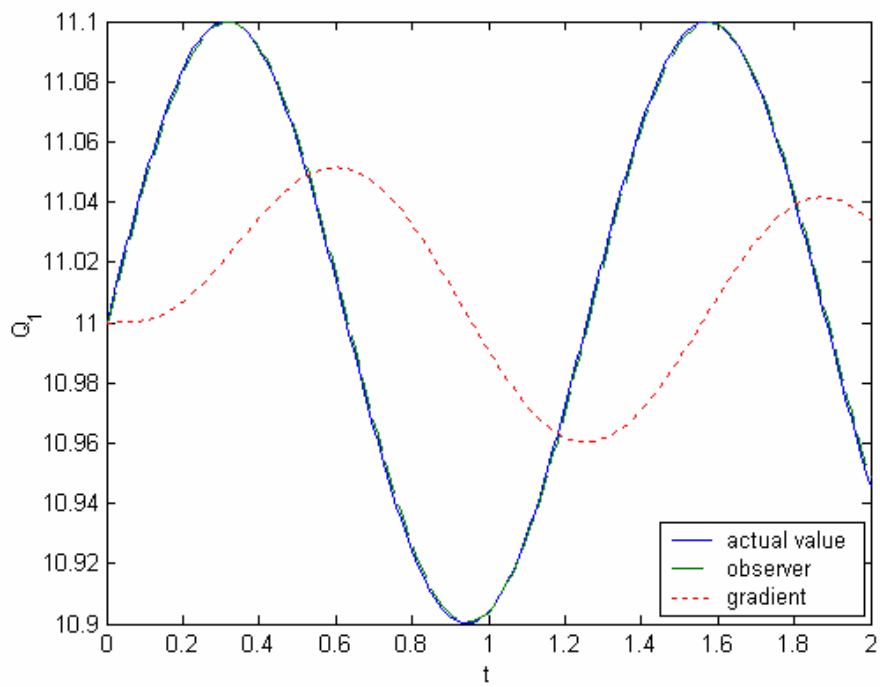and $k_1 = 10$, $Q_{1n} = 10.8$

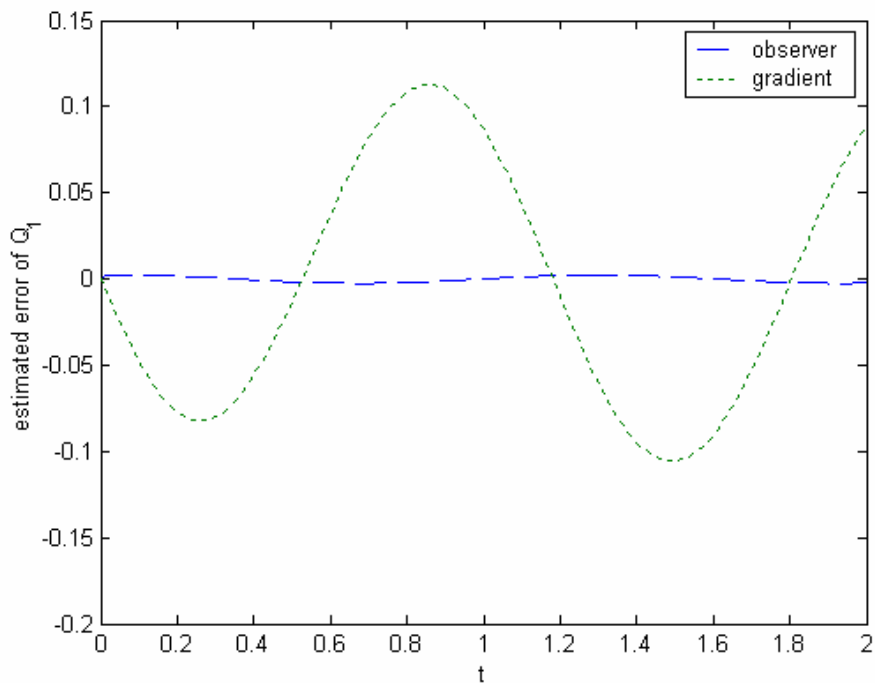Figure 4.20: Comparisons of estimators with observer approach and gradient method

Figure 4.21: Estimation errors of observer approach and gradient method

4.3 Adaptive Control System Design

In this section, we will employ the idea of adaptive control for voltage regulation of the power system. In practical, many dynamic systems to be controlled may have some uncertain parameters. In power system, it may be subjected to large variations in loading conditions. In this section, we may import the idea of adaptive control and use estimator as the load monitoring. We use the same VSC control law that be designed in Section 4.1; and use estimated parameter from estimator that be designed in Section 4.2 in the control law to achieve voltage regulation.

4.3.1 Control System Design

The basic idea of adaptive control is to estimate the uncertain plant parameters on-line based on the measured system signal, and use the estimated parameters in the control input computation. An adaptive control system can thus be regarded as a control system with on-line parameter estimation. It is known that the control and estimation can be designed separately and used together by separation principle.

In this section, we take the control law (Section 4.1) and implement it that using an estimated parameter of estimator (Section 4.2), the adaptive control system can be completed. The schematic of adaptive control power system is shown in Figure 4.22.
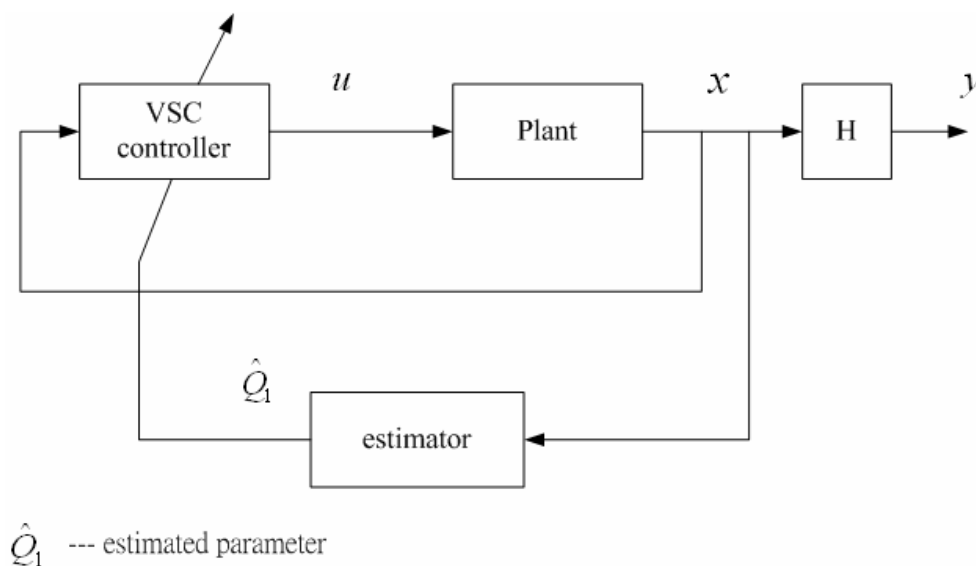

Figure 4.22: An adaptive control system

4.3.2 Application to Power Systems

As recalled in Section 4.1, we design VSC control law to achieve voltage regulation with

$$u = u^{eq} + u^{re} \tag{4.80}$$

$$u^{eq} = \frac{-g_1(x) - \sqrt{g_1(x)^2 - 4g_2(x)f(x)}}{2g_2(x)} \tag{4.81}$$

$$u^{re} = \frac{-\eta}{g_1(x) + 2g_2(x)u^{eq}} sgn(x_4 - 1) \tag{4.82}$$

where

$$f(x) = -7.03268 + 14.52288x_4 - 53.09608x_4^2 + (104.5752\cos(0.08727 - x_3)$$
$$+ 7.84314\sin(0.08727 - x_3))x_4 - 5.22876Q_1 - 7.03268$$

$$g_1(x) = 26.1438x_4\cos(0.08727 + x_1 - x_3) + 1.96079x_4\sin(0.08727 + x_1 - x_3)$$

$$g_2(x) = -26.21518x_4^2$$

If the reactive power demand of the load Q_1 is known exactly, we can use the above control law to achieve voltage regulation. However, we do not know the load variation of the power system exactly in practical.

In the next, let us assume that the load variation is not known exactly. We use estimator designing in Section 4.2 as the load monitoring to provide the estimated parameter $\hat{Q}_1$ to the controller. For true reactive power demand of the load Q_1 is constant, the estimated law is selected with

$$\hat{Q}_1 = k_1 e_1 + Q_{1n} \tag{4.83}$$

And for Q_1 is time varying with small variation, the estimated law is selected with

$$\hat{Q}_1 = Q_{1n} - k_1 e_1 + (\rho_1 + \eta_1)\, sat(\tfrac{e_1}{\phi_1}) \tag{4.84}$$

The voltage regulation performance may depend on the quality of the load estimates in the estimator.

In Section 4.1, we designed the VSC control law assuming that the true load variation is known. In the following simulations, the true parameter Q_1 is substituted for $\hat{Q}_1$. The schematic is shown in Figure 4.22. In Figure 4.23, the true reactive power demand of the load is assumed to be $Q_1 = 11.2$. The value of Q_{1n} is chosen to be 11. The initial state of the system is $x_0 = [0, 0, 0, 1.1]$, and the other design parameters are taken to be $k_1 = 10$, $\eta = 0.1$. Figure 4.23 (a) (b) show the estimating performance; Figure 4.23 (c) shows the result of voltage regulation, and the variation of tap changing ratio n is shown in Figure 4.23 (d). It is seen from Figure 4.23 (d), the VSC design using sign-type controller may lead to chattering. In practice, the chattering is undesirable. In order to eliminate chattering phenomenon, we can use saturation-type controller. We replace the controller of u the term $sgn(x_4 - 1)$ by $sat((x_4 - 1)/0.001)$. As shown in Figure 4.24, the chattering phenomenon has been improved. And Figure 4.25 shows the power system response with the VSC controller. Figure 4.26 shows the true reactive power demand of the load is a sinusoidal signal, $Q_1 = 11 + 0.1\sin(5t)$. The value of Q_{1n} is chosen to be 11. The initial state of the system is $x_0 = [0, 0, 0, 1.1]$, and the other design parameters are taken to be $k_1 = 1$, $\rho_1 = 0.2$, $\eta_1 = 0.01$, $\eta = 0.1$, $\phi_1 = 0.001$. Figure 4.26 shows the simulation result. The simulation results have demonstrated the effectiveness of our proposed adaptive scheme.
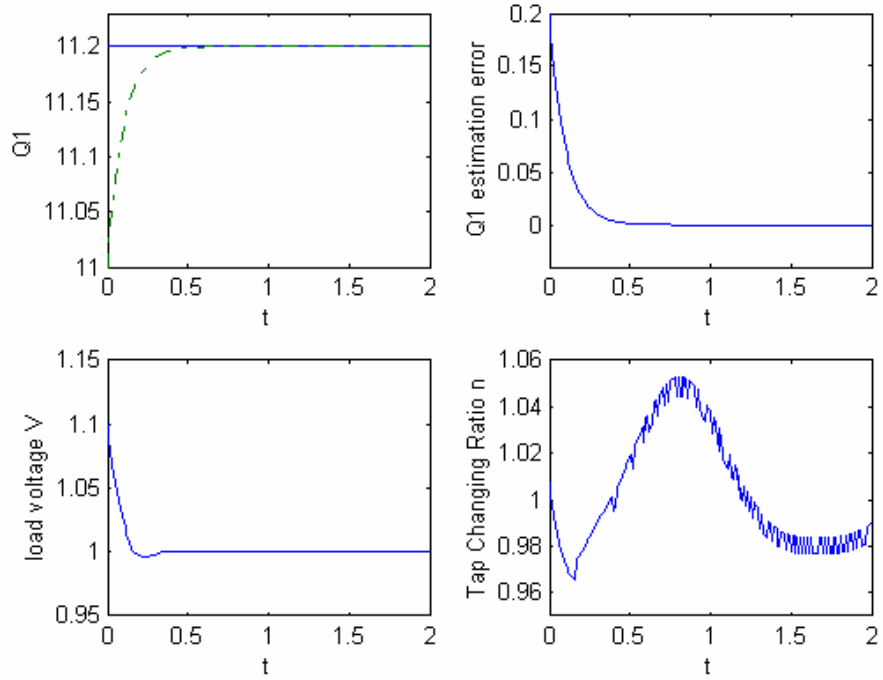
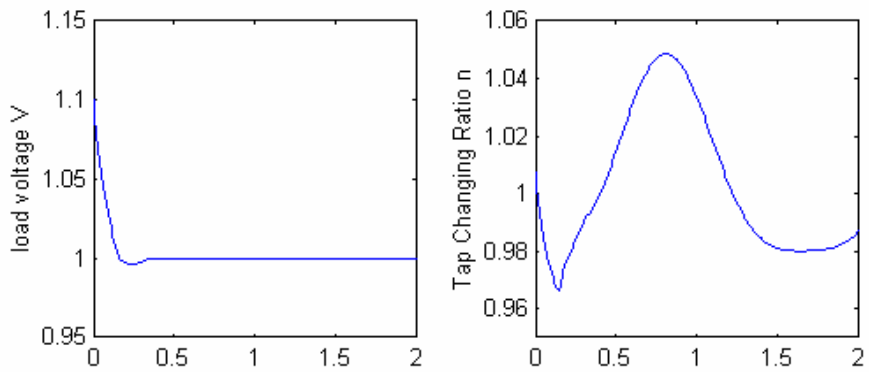Figure 4.23: Regulating performance and parameter estimation for $Q_1 = 11.2$

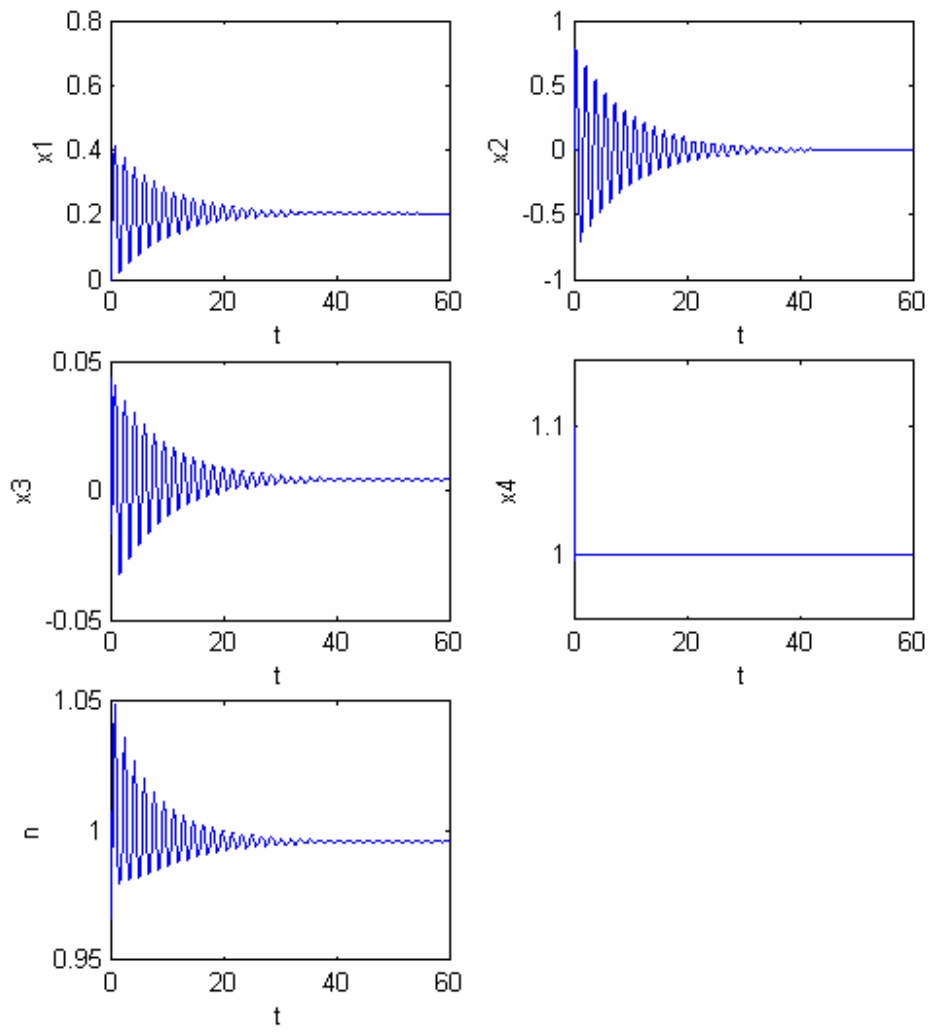Figure 4.24: Regulating performance with Saturation control input
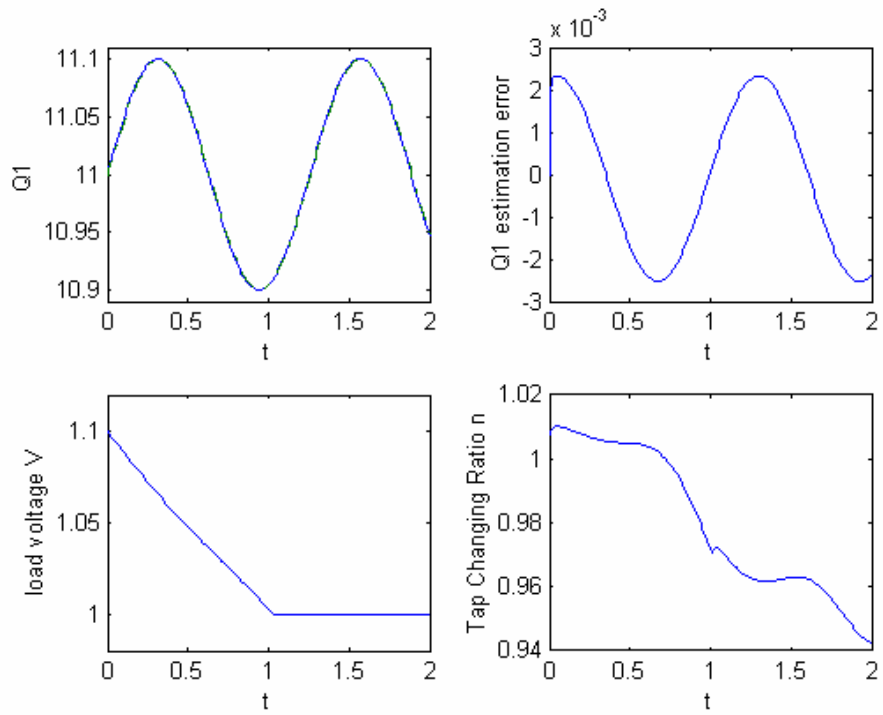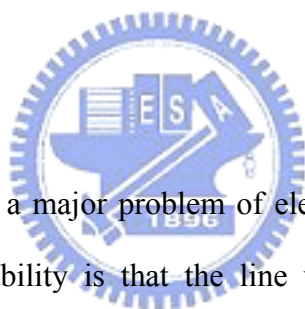
Figure 4.25: System response

Figure 4.26: Regulating performance and parameter estimation for

$$Q_1 = 11 + 0.1\sin(5t)$$

CHAPTER 5

Control of Voltage Collapse

As discussed in Chapter 3, a major problem of electric power system is "voltage collapse". This kind of instability is that the line voltage in PQ-load may jump sharply from the rated voltage to a deeply low voltage as PQ-load varies. In Chapter 3, we employ the FIDF design technique and signal analysis tool to the detection of voltage collapse in a power system. It is found that the voltage collapse can be successfully detected and generate the alarm signal by properly adjusting the threshold. With the announcement of warning signal, it is useful for us to initiate appropriate control actions to prevent such instability phenomena.

In Chapter 4, we focus on the design of Variable Structure Control law to achieve voltage regulation for the electric power system. By utilizing tap changer to regulate the voltage level and raise the electric quality of the electric power system. Besides, we also design a parameter estimator as the load monitor to provide the load variation of the power system. It provides the accurate parameter variation to the controller to

have better regulating capacity. It also make controller to be able to deal with the existence of parameter uncertainty in a system. In this chapter, we will show a design of prevention of voltage collapse by employing prior designs.

5.1   Control of Voltage Collapse

The effect of the tap changer ratio of the power system is that the system Hopf range can be decreased or even eliminated by suitable changing tap changer ratio. Further, with the existence of power system equilibria, it is found that the power system stable region can be enlarged by changing tap changer ratio. Moreover, the control of Hopf bifurcation is also a good design of prevention of voltage collapse. The details are discussed in [39].

In Chapter 3, we succeed to develop a means to detect the occurrence of voltage collapse in a power system and to generate a warning signal to admonish us. We also find that we can regulate the voltage level to raise the electric quality of the electric power system by utilizing tap changer in Chapter 4. Here, we will utilize the tap changer to prevent the occurrence of voltage collapse at the time of the detected equipment send out a warning signal. A detail scheme is shown in Figure 5.1.
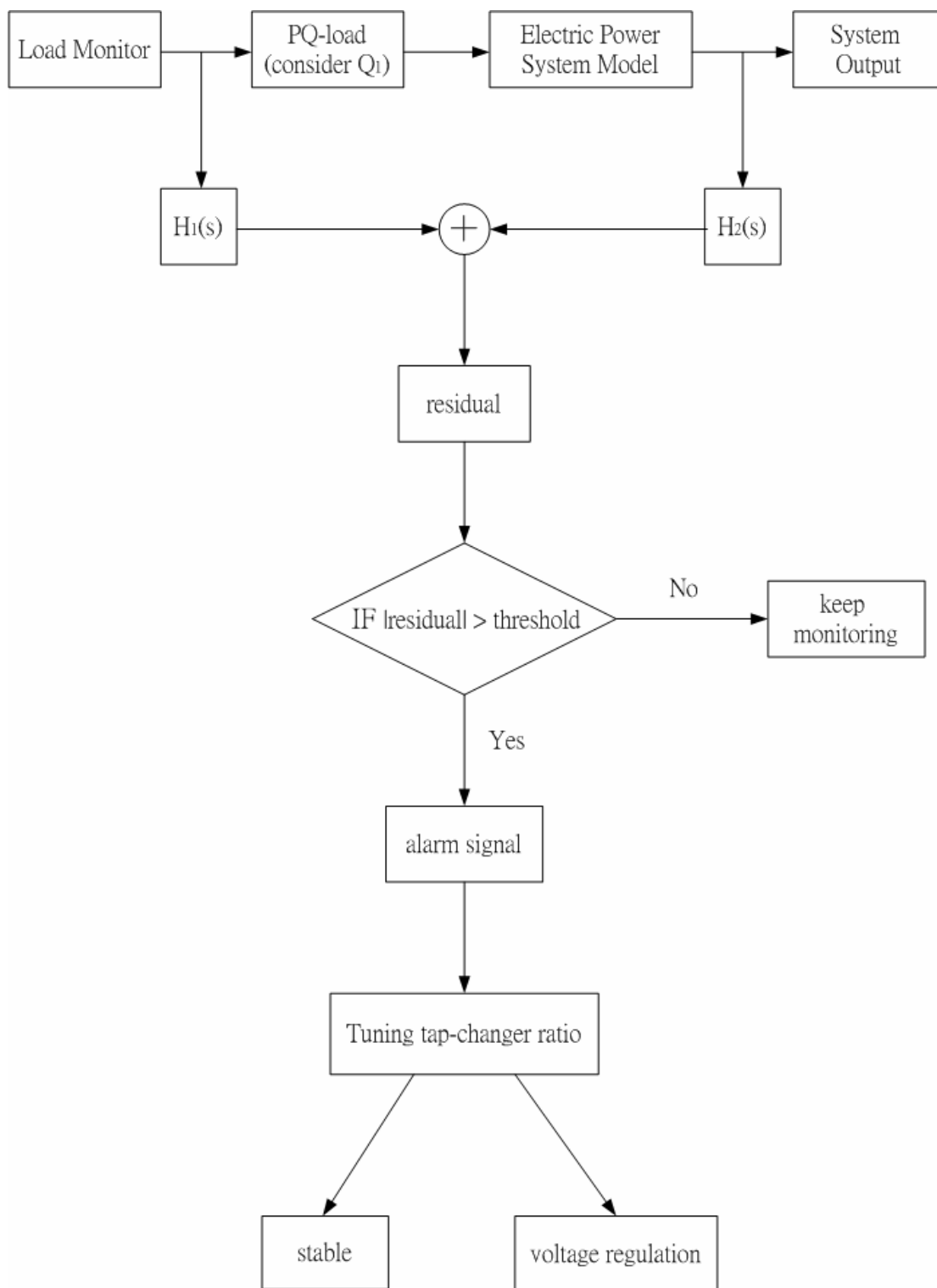
Figure 5.1: A scheme of prevention of voltage collapse

5.2 Simulation Results

Figures 5.2-5.3 show two examples of proposed scheme. In these simulations, the system initial state is $x_0 = [0, 0, 0, 1.1]$, the reactive power demand of the load is $Q_1 = 11.3$. It makes the power system operation exceeding its stability limit. It is observed from Figure 5.2(b) and 5.3(b) that the system undergoes voltage collapse for such heavy load. Figure 5.2(b) shows the load voltage collapse around t=1.13. However, by properly adjusting the threshold, we can detect it before it occurs. In these simulations, we select threshold to be 0.06 p.u. As displayed in Figure 5.2(d) and 5.3(d), the voltage collapse can be successfully detected and the alarm signal is fired before t=1. It makes us having enough time to take a proper control action to avoid such instability. In Figure 5.2(e), we increase tap changer ratio to enlarge the power system stable region. It is found in Figure 5.2(f) that the voltage collapse behavior disappears and the load voltage reaches a new equilibrium point after a transient of oscillation. Furthermore, we shall employ the VSC control law designing in section 4.1 to achieve regulating the load voltage. This can be seen from Figure 5.3(e) and Figure 5.3(f). Simulation results have demonstrated the effectiveness of our proposed scheme of prevention of the voltage collapse.

Figure 5.2: (a) load variation (Q_1) (b) time response of load voltage without control

(c) residual signal   (d) alarm signal by FIDF   (e) tap changer ratio n
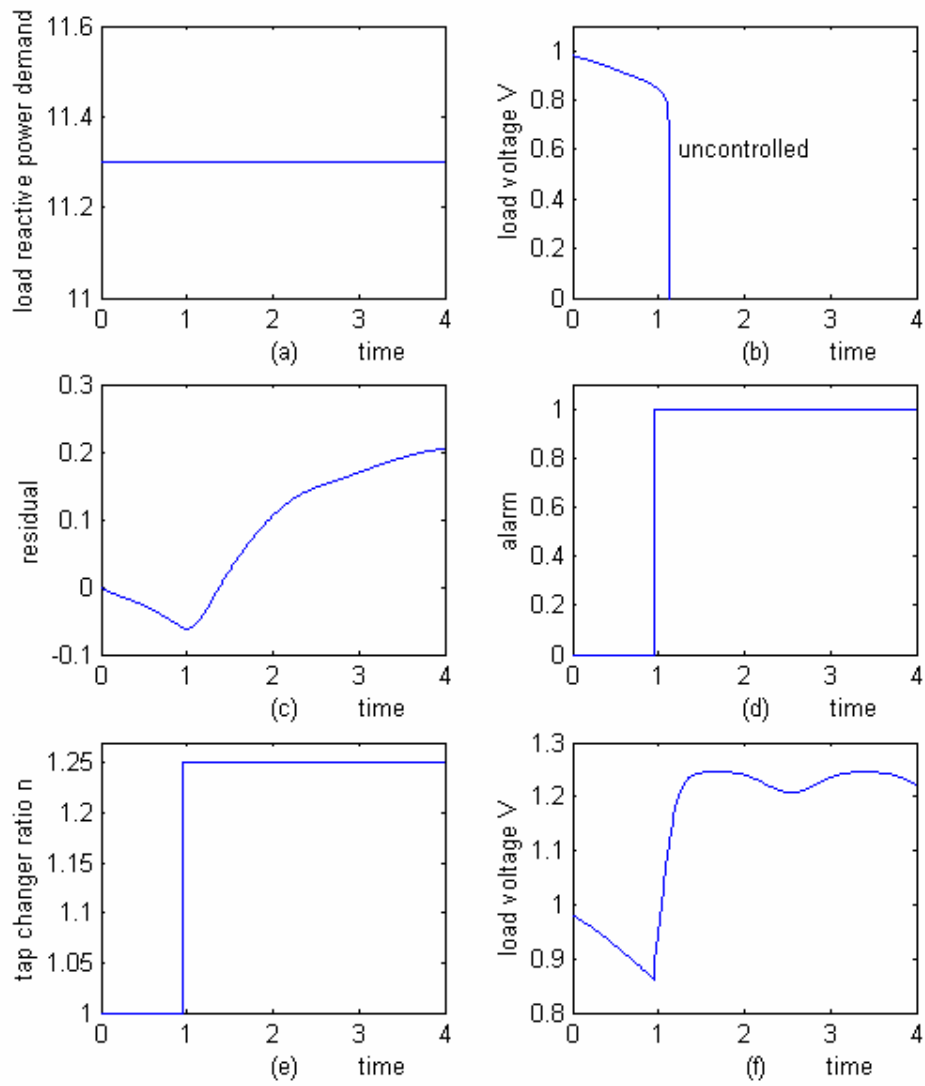
(f) time response of load voltage with control given by (e)
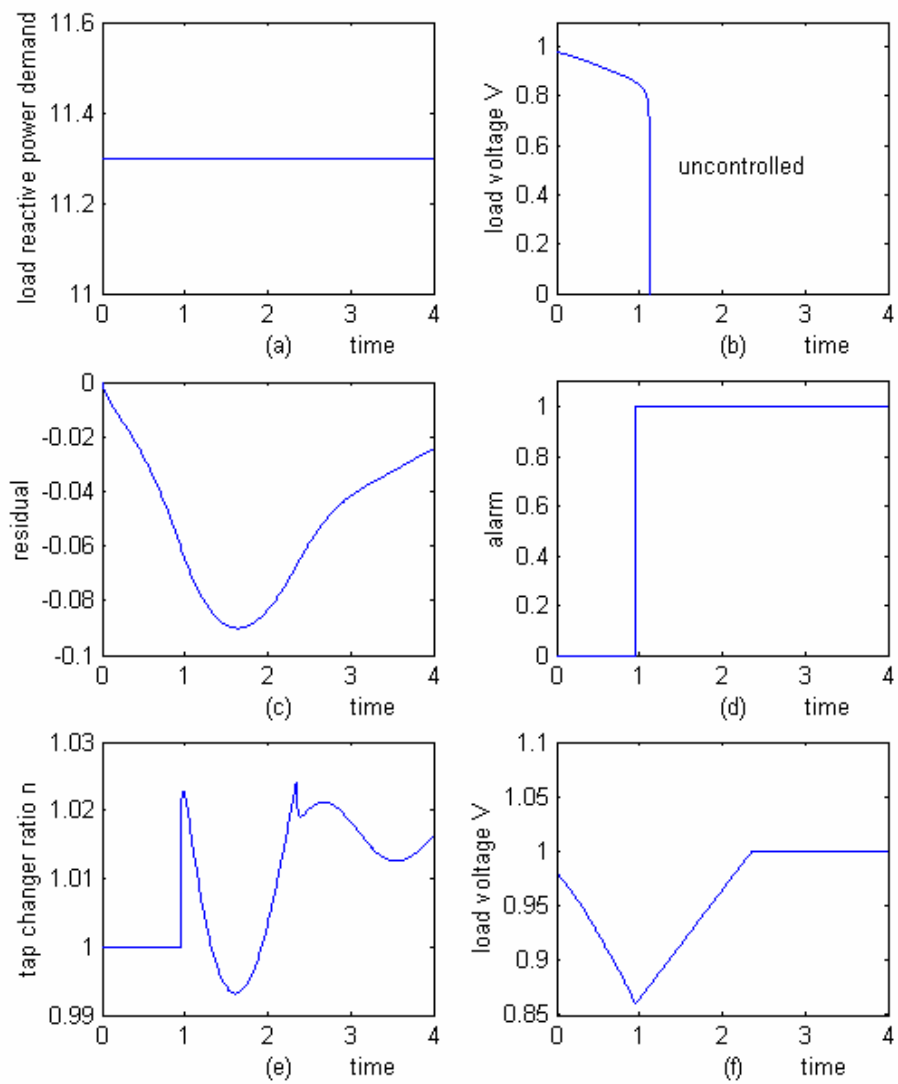
Figure 5.3: (a) load variation (Q_1) (b) time response of load voltage without control

(c) residual signal (d) alarm signal by FIDF

(e) variation of tap changer ratio n

(f) time response of load voltage with control given by (e)

CHAPTER 6

Conclusions and Suggestions for Further Research

In this thesis, we have studied the detection of voltage collapse using a Dobson and Chiang's power system model. By treating the difference between the output of the power system model and that of its linearized model as a fault vector and employing a FIDF design technique, the occurrence of voltage collapse is shown to be successfully detected by inspecting the residual signal generated from the FIDF. The performance of detecting voltage collapse depends on the setting of the threshold. Simulations in Chapter 3 are given to demonstrate the effectiveness of this approach.

To raise the voltage quality of power supply for satisfactory operation of a power system, we add an extra tap changer parallel to the nonlinear load to Dobson and Chiang's power system model. We have applied Variable Structure Control design scheme to adjust the tap changer ratio to achieve voltage regulation. According to the

simulations in Section 4.1, it is shown that the designed controller can achieve the desired performance. However, in practical power system, the system dynamics may have well known dynamics at the beginning, but will experience unpredictable load variation as the control operation goes on. For this reason, we have proposed a parameter estimator as the load monitor to provide the load variation of the power system in Section 4.2. It provides the accurate load variation to the VSC voltage controller to have better regulating capacity.

To prevent the voltage collapse, we have proposed a scheme of prevention of voltage collapse based on prior designs. We utilize the tap changer to prevent the occurrence of voltage collapse. At the time of the detected equipment send out a warning signal, we tune the tap changer ratio to prevent the occurrence of voltage collapse. Further, we have employed the VSC controller to regulate the load voltage. Simulations in Chapter 5 demonstrate the effectiveness of this scheme.

In the following, we indicate some directions for further research. Firstly, for detection of voltage collapse, we provide a means for quick detection of voltage collapse but not the only one. Recently, the issue of detecting voltage collapse has attracted more and more attention [12,14,30]. It is a way for further research. Secondly, for voltage control, in addition to the use of Tap changer, another feasible means can also be added, such as shunt capacitors or series capacitors. To consider voltage control with capacitors is also a direction of study. Finally, in this thesis, we focus on voltage control. However, an efficient and reliable operation of power systems should have the property that the voltage and frequency should remain nearly constant. Thus, the final direction is frequency control.

References

[1] Abed, E. H., Hamdan, A. M. A., Lee, H. C., and Parlos, A. G., "On bifurcations in power system models and voltage collapse," *Proc. of the 29th IEEE Conference on Decision and Control* , Vol. 6, Dec. 1990, pp.3014-3015.

[2] Abed, E. H., Alexander, J. C., Wang, H., Hamdan, A. M. A., and Lee, H. C., "Dynamic bifurcations in a power system model exhibiting voltage collapse," *IEEE International Symposium on Circuits and Systems*, Vol. 5, May 1992, pp. 2509-2512.

[3] Bacciotti, A., *Local Stabilizability of Nonlinear Control system*, World Scientific Publishing, Co. Pte. Ltd., 1992.

[4] Canizares, C.A., De Souza, A.C.Z., and Quintana, V.H., "Comparison of performance indices for detection of proximity to voltage collapse," *IEEE Transactions on Power Systems*, Vol. 11, Issue: 3, Aug. 1996, pp. 1441-1450.

[5] Chang, S. K. and Hsu, P. L., "Design the fault identification filter via a simplified transfer matrix approach," *Proc. of the American Control Conference*, 1992, pp. 2119-2120.

[6] Chow, J. H. and Gebreselassie, A., "Dynamic voltage stability analysis of a single machine constant power load system," *Proc. of the 29th IEEE Conference on Decision and Control*, Vol. 6, Dec. 1990, pp. 3057-3062.

[7] Ding, X. and Frank, P.M., "Fault detection via factorization approach," *Systems and Control Letters*, Vol. 14, 1990, pp. 431-436.

[8] Dobson, I., Chiang, H. D., Thomas, R. J., Thorp, J. S., and Fekih-Ahmed, L., "On voltage collapse in electric power systems," *IEEE Transactions on Power Systems*, Vol. 5, 1990, pp. 601-611.

[9] Dobson, I., Chiang, H. D., Thorp, J. S., and Fekih-Ahmed, L., "A model of voltage collapse in electric power systems," *Proc. of the 27th IEEE Conference on Decision and Control*, Vol.3, Dec. 1988, pp.2104-2109.

[10] Gao, L., Chen, L., Fan, Y., and Ma, H., "A nonlinear control design for power systems," *Automatica*, Vol. 28, 1992, pp. 975-979.

[11] Goswami, J. C. and Chan, A. K., *Fundamentals of wavelets: theory, algorithms , and applications*, New York, Wiley, 1999.

[12] Huang, G.M. and Nair, N.-K.C., "Detection of dynamic voltage collapse," *IEEE Power Engineering Society Summer Meeting*, Vol. 3, July 2002, pp. 1284-1289.

[13] Jiang, F., Choi, S.S., and Shrestha, G., "Power system stability enhancement using static phase shifter," *IEEE Transactions on Power Systems,* Vol. 12, Issue: 1, Feb. 1997, pp. 207-214.

[14] Ke Chen, Hussein, A., Bradley, M.E., and Wan, H., "A performance-index guided continuation method for fast computation of saddle-node bifurcation in power systems," *IEEE Transactions on Power Systems,* Vol. 18, Issue: 2, May 2003, pp. 753-760.

[15] Koo, K. M. and Kim, J. H., "Robust control of robot manipulators with parametric uncertainty," *IEEE Transactions on Automatic Control,* Vol. 39, Issue: 6, June 1994, pp. 1230-1233.

[16] Kundur, P., *Power System Stability and Control*, McGraw-Hill, Inc., 1994.

[17] Lee, B. H. and Lee, K. Y., "A study on voltage collapse mechanism in electric power systems," *IEEE Transactions on Power Systems,* Vol. 6, Issue: 3, Aug. 1991, pp. 966-974.

[18] Liang, Y. W. and Liaw, D. C., "Application of FIDF to the detection of unstable behavior in compression systems," *Proc. of the 39th Conference on Decision and Control*, Vol. 2, Dec. 2000, pp. 1347-1352.

[19] Liang, Y. W. and Liaw, D. C., "Detection of surge and stall in compression systems: an example study," *IEEE Transactions on Automatic Control*, Vol. 46, No. 10, 2001, pp. 1609-1613.

[20]   Liu, C. C. and Vu, K.T., "Analysis of tap-changer dynamics and construction of voltage stability regions," *IEEE Transactions on Circuits and Systems,* Vol. 36, Issue: 4, April 1989, pp. 575-590.

[21]   Lof, P. A., Smed, T., Andersson, G., and Hill, D.J., "Fast calculation of a voltage stability index," *IEEE Transactions on Power Systems,* Vol. 7, Issue:1, Feb. 1992, pp. 54-64.

[22]   Ohtsuki, H., Yokoyama, A., and Sekine, Y., "Reverse action of on-load tap changer in association with voltage collapse," *IEEE Transactions on Power Systems,* Vol. 6, Issue: 1, Feb. 1991, pp. 300-306.

[23]   Park, J., Rizzoni, G., and Ribbens, W. B. "On the representation of sensors fault detectionfilters," *Proc. of the 32nd IEEE Conference on Decision and Control*, Vol. 2, 1993, pp. 1728-1732.

[24]   Roumeliotis, S. I., Sukhatme, G. S., and Bekey, G. A., "Fault detection and Identification in a Mobile Robot using Multiole-Model Estimation," *Proc. of the IEEE international Conference on Robotics & Automation,*Vol. 3, 1998, pp. 2223-2228.

[25]   Slotine, J.-J. E. and Li, W., *Applied Nonlinear Control,* Prentice-Hall, Englewood Cliffs, NJ, 1991.

[26]   Su, C. Y. and Leung, T. P., "A sliding mode controller with bound estimation for robot manipulators," *IEEE Transactions on Robotics and Automation*, Vol. 9, Issue: 2, April 1993, pp. 208-214.

[27]   Taylor, C.W., *Power System Voltage Stability*, McGraw-Hill, Inc., 1994.

[28]   Thomas, R. J. and Tiranuchit, A., "Dynamic voltage instability," *IEEE Proc. of 26th Conference on Decision and Control*, Dec. 1987.

[29]   Utkin, V. I., *Sliding modes and their application to variable structure systems*, MIR Publishers, Moscow, Russia, 1978.

[30] Verbic, G. and Gubina, F., "A novel concept for voltage collapse protection based on local phasors," *Transmission and Distribution Conference and Exhibition : Asia Pacific. IEEE/PES*, Vol. 1, Oct. 2002, pp. 124-129.

[31] Walve K., "Modelling of Power System Components at Severe Disturbances," CIGRE paper 38-18, *International Conference on Large High Voltage Electric Systems*, Aug. 1986.

[32] Wang, H.O., Abed, E.H., and Hamdan, A.M.A., "Bifurcations, chaos, and crises in voltage collapse of a model power system," *IEEE Transactions on Circuits and Systems I: Fundamental Theory and Applications*, Vol. 41, Issue: 4, April 1994, pp. 294-302.

[33] Wang, Y., Hill, D.J., Middleton, R.H., and Gao, L., "Transient stability enhancement and voltage regulation of power systems," *IEEE Transactions on Power Systems,* Vol. 8, Issue: 2, May 1993, pp. 620-627.

[34] Wang, Y., Mohler, R.R., Spee, R., and Mittelstadt, W., "Variable-structure facts controllers for power system transient stability," *IEEE Transactions on Power Systems,* Vol. 7, Issue: 1, Feb. 1992, pp. 307-313.

[35] Xu, W. and Mansour, Y., "Voltage stability analysis using generic dynamic load models," *IEEE Transactions on Power Systems,* Vol. 9, Issue: 1, Feb. 1994, pp. 479-493.

[36] Yijia Cao, Lin Jiang, Shijie Cheng, Deshu Chen, Malik, O.P., and Hope, G.S., "A nonlinear variable structure stabilizer for power system stability," *IEEE Transactions on Energy Conversion*, Vol. 9, Issue: 3, Sept. 1994, pp. 489-495.

[37] Young Huei Hong, Ching Tsai Pan, and Wen Wei Lin, "Fast calculation of a voltage stability index of power systems," *IEEE Transactions on Power Systems,* Vol. 12, Issue: 3, Nov. 1997, pp. 1555-1560.

[38] Zhu, Chunlei, Zhou, Rujing, and Wang, Yonyi, "A new decentralized nonlinear voltage controller for multimachine power systems," *IEEE Transactions on Power Systems,* Vol. 13, Feb. 1998, pp. 211-216.

[39]　方冠勳，*電力系統加入電壓調整器之分叉特性分析與控制*，國立交通大學，碩士論文，1995.